

# Simultaneous Multiphase Flash and Stability Analysis Calculations Including Solid CO<sub>2</sub> for CO<sub>2</sub>–CH<sub>4</sub>, CO<sub>2</sub>–CH<sub>4</sub>–N<sub>2</sub>, and CO<sub>2</sub>–CH<sub>4</sub>–N<sub>2</sub>–O<sub>2</sub> Mixtures

Giorgia De Guido\* and Elvira Spatolisano

Cite This: *J. Chem. Eng. Data* 2021, 66, 4132–4147

Read Online

ACCESS |



Metrics &amp; More



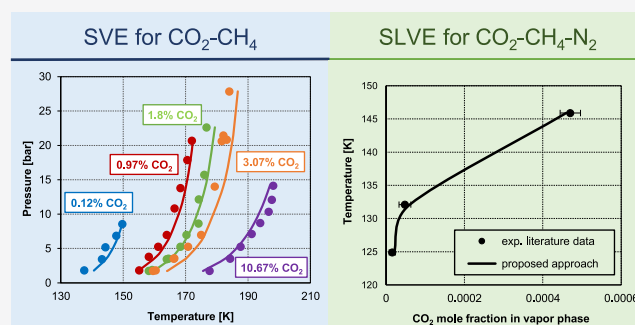
Article Recommendations



Supporting Information

**ABSTRACT:** This work deals with solid–vapor equilibria and solid–liquid–vapor equilibria of carbon dioxide in mixtures of interest for natural gas purification and biogas upgrading. Experimental data available in the literature are reviewed and an algorithm for solving an isobaric–isothermal flash coupled to a phase stability analysis is presented, which does not require *a-priori* knowledge of the number and type of phases existing at equilibrium. The good agreement between calculation results, also performed with a tool that makes use of Gibbs free energy minimization, and experimental data suggests that the proposed approach can be used for determining suitable operating conditions for processes aimed at separating CO<sub>2</sub> out of a gas by freezing it.

This work points out that more experimental studies should be performed on phase equilibria in the presence of solid CO<sub>2</sub> for multicomponent mixtures containing species other than methane (e.g., nitrogen and oxygen), which are representative of gaseous streams from which CO<sub>2</sub> needs to be removed, such as natural gas, biogas, and flue gas from power plants. Such data are important for a proper calibration of thermodynamic models that must be selected for reliable process simulations.



## 1. INTRODUCTION

In the process industry field, one of the biggest concerns has always been the sweetening of acid gaseous streams. During the last decades, various technologies have been studied and tested in order to efficiently reduce the amount of acid components in these streams. In particular, attention has been focused on carbon dioxide removal. In fact, CO<sub>2</sub> is considered as one of the most significant greenhouse gases, and its increasing concentration in the atmosphere plays a major role in increasing global warming. Moreover, the presence of high CO<sub>2</sub> contents in natural gas results in a reduction of the calorific value of the gas and causes corrosion of the pipeline and equipment, along with many other operational problems.<sup>1</sup> Among the established CO<sub>2</sub> separation strategies, recently CO<sub>2</sub> capture using low-temperature/cryogenic technologies has received increasing attention. Previous works have demonstrated they have lower energy consumptions than conventional amine scrubbing if applied both to natural gas purification<sup>2</sup> and to biogas upgrading.<sup>3</sup> Another advantage these technologies offer is that pure CO<sub>2</sub> is separated as a liquid under pressure rather than in the gaseous state at near ambient pressure, thus making it relatively easy to pump underground for storage or to be used for enhanced oil recovery (EOR) applications.<sup>4</sup>

This has boosted an intense research activity on measurement and thermodynamic modeling of CO<sub>2</sub> frost points and

other types of phase equilibria involving solid CO<sub>2</sub> in natural gas or biogas mixtures. Both activities are important to correctly describe the thermodynamic behavior of the system of interest, which in turn plays a key role in the design of novel low-temperature/cryogenic processes.

The aim of this work is 2-fold. First of all, it focuses on the solid–vapor equilibrium (SVE) and solid–liquid–vapor equilibrium (SLVE) experimental data available in the literature for systems containing CO<sub>2</sub> and methane, nitrogen, and oxygen. In section 2, for each data set, the following information is reported (when available): the experimental procedure, the mixture composition or the range of CO<sub>2</sub> concentrations, the temperature and pressure range, and the number of points. Then, in section 3, an algorithm is presented for the simultaneous computation of phase stability and multiphase equilibria of CO<sub>2</sub>-containing mixtures. Section 4 presents the results of the calculations, which are also compared with those given by another tool that makes use of Gibbs free energy minimization.

**Special Issue:** In Honor of A. E. Mather

**Received:** April 30, 2021

**Accepted:** August 6, 2021

**Published:** September 1, 2021



Table 1. SVE Experimental Data Available in the Literature for the CO<sub>2</sub>–CH<sub>4</sub> System

lit. source	measurement technique	data type	mixture	T [K]	P [bar]	no. points
Pikaar (1959) <sup>6</sup>	nonsampling technique	frost points ( <i>T</i> , <i>P</i> )	1 to 20 mol % CO <sub>2</sub>	158.25 to 210.48	1.966 to 48.322	38
	sampling technique	<i>P</i> , <i>x</i> <sub>CO<sub>2</sub>,V</sub> at 7 temperatures	not available <sup>a</sup>	133.15 to 210.15	1.56 to 47.896	66
Agrawal and Laverman (1995) <sup>8</sup>	nonsampling visual technique	frost points ( <i>T</i> , <i>P</i> ) for 5 mixtures	0.12 to 10.67 mol % CO <sub>2</sub>	137.54 to 198.09	1.724 to 27.855	42
Le and Trebble (2007) <sup>7</sup>	nonsampling visual technique	frost points ( <i>T</i> , <i>P</i> ) for 3 mixtures	1.00 to 2.93 mol % CO <sub>2</sub>	168.6 to 187.7	9.621 to 30.082	55
Zhang et al. (2011) <sup>9</sup>	isochoric method	frost points ( <i>T</i> , <i>P</i> ) for 5 mixtures	10.8 to 54.2 mol % CO <sub>2</sub>	191.1 to 210.3	2.93 to 44.46	17
Xiong et al. (2015) <sup>11</sup>	static analytic method with sampling technique	SVE ( <i>T</i> , <i>P</i> , <i>x</i> <sub>CO<sub>2</sub>,V</sub> ) at 6 temperatures	0.5 to 20.1 mol % CO <sub>2</sub>	153.15 to 193.15	2.19 to 30.38	64

<sup>a</sup>The global composition of the mixture for which solid–vapor equilibrium conditions were determined experimentally by Pikaar<sup>6</sup> using the saturation cell apparatus is not given in his Ph.D. thesis, where it is reported that at the beginning of the experiment the walls of the saturation cell were coated with solid CO<sub>2</sub> and this solid saturated the methane flowing through the cell from the storage.

## 2. EXPERIMENTAL DATA

This section deals with the available literature concerning phase equilibria in the presence of solid CO<sub>2</sub>, focusing on CO<sub>2</sub>–CH<sub>4</sub> mixtures and on ternary and quaternary mixtures that also contain N<sub>2</sub> and O<sub>2</sub>. The latter systems are of interest considering that nitrogen is a classical natural gas impurity<sup>5</sup> and, in some cases, air is present in the raw biogas (e.g., in biogas produced in landfills).

Data for the temperature and pressure are reported in Kelvin and in bar, respectively. Therefore, the data available in the literature have been converted when reported in different units of measurement. The global composition of the analyzed mixtures is also reported, when available.

**2.1. The CO<sub>2</sub>–CH<sub>4</sub> system.** Table 1 summarizes the SVE data available in the literature for the CO<sub>2</sub>–CH<sub>4</sub> system, which are organized on the basis of their literature source. Detailed data are reported in Tables S1–S6 in the Supporting Information.

In his Ph.D. thesis work, Pikaar<sup>6</sup> determined the phase equilibria of the CO<sub>2</sub>–CH<sub>4</sub> system using two methods. A nonsampling technique was used to determine frost points of mixtures with a CO<sub>2</sub> content ranging from 1 to 20 mol %, while a sampling method was used to determine the composition of the vapor phase in equilibrium with solid CO<sub>2</sub> at temperatures from 133.15 to 210.15 K. Le and Trebble<sup>7</sup> observed there exist slight variances in Pikaar's two data sets, especially at lower CO<sub>2</sub> concentrations.

Agrawal and Laverman<sup>8</sup> used a nonsampling visual technique in which a known gas mixture of CO<sub>2</sub>–CH<sub>4</sub> was charged into the cell (i.e., the cryostat), and the pressure and temperature at which the solid phase just began to form were determined. Their data included frost point measurements for five different binary mixtures of CO<sub>2</sub> and CH<sub>4</sub> containing, respectively, 0.12 mol % CO<sub>2</sub>, 0.97 mol % CO<sub>2</sub>, 1.8 mol % CO<sub>2</sub>, 3.07 mol % CO<sub>2</sub>, and 10.67 mol % CO<sub>2</sub>.

Le and Trebble<sup>7</sup> pointed out there is considerable disagreement at higher pressures (at which natural gas processing plants are usually operated) for the SVE data presented in the years before in the above-mentioned literature works. In an attempt to reconcile these differences, they used a nonsampling technique to perform frost point measurements on three different CO<sub>2</sub>–CH<sub>4</sub> mixtures containing, respectively, 1.00 mol % CO<sub>2</sub>, 1.91 mol % CO<sub>2</sub>, and 2.93 mol % CO<sub>2</sub> at 9.621 to 30.082 bar and 168.6 to 187.7 K.

Some years later, Zhang and co-workers<sup>9</sup> presented new experimental data for the frost points of CO<sub>2</sub>–CH<sub>4</sub> mixtures covering a wide range of CO<sub>2</sub> concentrations, from 10.8 to 54.2 mol % CO<sub>2</sub>. Thus, they extended the analysis performed in previous years to systems of interest when considering the removal of CO<sub>2</sub> from high carbon dioxide-content natural gas fields, which is important to the gas industry development in some countries (e.g., Indonesia and Malaysia).<sup>10</sup>

The work by Xiong et al.<sup>11</sup> provides CO<sub>2</sub> SVE data over a wide range of composition, temperature, and pressure in the region of practical application for the natural gas industry. The method to collect phase equilibrium data was the static analytic method with sampling technique, thus providing the composition of the vapor phase at equilibrium.

Table 2 summarizes the SLVE data available in the literature for the CO<sub>2</sub>–CH<sub>4</sub> mixture, which is well-known to exhibit a SLVE locus that passes through a maximum in the *P* vs *T* diagram. Detailed data are reported in Tables S7–S14 in the Supporting Information. In Table 2, the data from Shen et al.<sup>12</sup> and Gao et al.<sup>13</sup> are not considered, since they are presented as SLE data, though Riva and Stringari<sup>14</sup> observed they are actually SLVE data for which only the CO<sub>2</sub> mole fraction in the liquid phase was reported.

Donnelly and Katz<sup>15</sup> presented data in terms of temperature and pressure pairs along the SLVE locus. In addition to that, they also showed two isobaric temperature–composition diagrams (at 500 and 673 psia, respectively, as shown in Figure S1 in the Supporting Information), which can be used to obtain another four *T*, *P* conditions at which SLVE establishes for the system CO<sub>2</sub>–CH<sub>4</sub>.

The experimental work by Sterner<sup>16</sup> was undertaken as a result of the need to extend the work done by Donnelly and Katz<sup>15</sup> to low temperatures. The data presented are of particular interest because they differ considerably from some of the results presented by Donnelly and Katz,<sup>15</sup> especially their extrapolation of SLVE points to lower temperatures.

The experimental work by Davis and co-workers<sup>17</sup> was carried out to determine the SLV phase behavior of the CO<sub>2</sub>–CH<sub>4</sub> mixture at CO<sub>2</sub> concentrations commonly encountered in natural gas.

Im and Kurata<sup>18</sup> summarized the data reported by Davis et al.<sup>17</sup> and Brewer and Kurata<sup>19</sup> concerning the SLV locus of the CO<sub>2</sub>–CH<sub>4</sub> system.

**2.2. The CO<sub>2</sub>–CH<sub>4</sub>–N<sub>2</sub> system.** As previously pointed out, since nitrogen may be present in the gaseous streams to be

**Table 2. SLVE Experimental Data Available in the Literature for the CO<sub>2</sub>–CH<sub>4</sub> System**

lit. source	data type	T [K]	P [bar]	no. points
Donnelly and Katz (1954) <sup>15</sup>	T, P	191.76 to 215.65	9.170 to 48.539	25 <sup>a</sup>
Sterner (1961) <sup>16</sup>	T, P	166.43 to 199.93	19.472 to 49.887	6 <sup>b</sup>
	T–x <sub>CO<sub>2</sub>V</sub>	166.5 to 202.4	19.305 to 49.987	8 <sup>c</sup>
	T–x <sub>CO<sub>2</sub>L</sub>	166.9 to 177.7	19.305 to 28.958	3 <sup>c</sup>
Davis et al. (1962) <sup>17</sup>	T, P	97.54 to 211.71	0.283 to 48.677	38
	T–x <sub>CO<sub>2</sub>V</sub>	140.93 to 205.71	6.895 to 48.263	8 <sup>d</sup>
	T–x <sub>CO<sub>2</sub>L</sub>	129.65 to 201.26	3.447 to 48.263	11 <sup>d</sup>
Im and Kurata (1971) <sup>18</sup>	T–P–x <sub>CO<sub>2</sub>V</sub> –x <sub>CO<sub>2</sub>L</sub>	165.21 to 210.21	18.961 to 48.470	10

<sup>a</sup>Including the four T, P conditions that can be read from the two isobaric temperature–composition diagrams (at 500 and 673 psia, respectively, as shown in Figure S1 in the Supporting Information) reported by Donnelly and Katz.<sup>15</sup> <sup>b</sup>Obtained from the P vs T plot reported by Sterner.<sup>16</sup> <sup>c</sup>Obtained from the T–composition plot reported by Sterner.<sup>16</sup> The pressure ranges reported for these two data sets have been inferred considering the temperature range they refer to and with the aid of the P vs T plot reported by Sterner.<sup>16</sup> <sup>d</sup>The pressure ranges reported for these two data sets have been inferred considering the temperature range they refer to and with the aid of the P vs T plot reported by Davis et al.<sup>17</sup>

treated for removing CO<sub>2</sub> by low-temperature/cryogenic technologies, it is important to collect phase equilibrium data in the presence of solid CO<sub>2</sub> also for this ternary mixture. Agrawal and Laverman,<sup>8</sup> Le and Trebble,<sup>7</sup> and Xiong et al.<sup>11</sup> performed frost point measurements for this ternary system, whereas SLVE was investigated by Riva and Stringari.<sup>14</sup> Table 3 summarizes the data available in the literature. More details on SVE data are reported in Tables S15–S18 in the Supporting Information. In Table 3, the data from Shen et

al.<sup>12</sup> and Gao et al.<sup>13</sup> are not reported, since they are presented as SLE data, though Riva and Stringari<sup>14</sup> observed they are actually SLVE data for which only the CO<sub>2</sub> mole fraction in the liquid phase was reported.

Focusing on frost point data first, Agrawal and Laverman<sup>8</sup> performed measurements on two CO<sub>2</sub>–CH<sub>4</sub>–N<sub>2</sub> mixtures having a composition similar to that of typical natural gases with a low content of CO<sub>2</sub>. The authors also reported some frost point data published by Haufe et al.<sup>20</sup> for two mixtures of the three components richer in N<sub>2</sub> (ca. 63 mol %), which are also included in Table 3.

CO<sub>2</sub> frost point data for the CO<sub>2</sub>–CH<sub>4</sub>–N<sub>2</sub> system were also collected by Le and Trebble<sup>7</sup> for mixtures containing 1 mol % and 1.95 mol % N<sub>2</sub>.

To investigate the influence of nitrogen on the CO<sub>2</sub> frost points, two types of CO<sub>2</sub>–CH<sub>4</sub>–N<sub>2</sub> ternary mixtures were investigated by Xiong et al.<sup>11</sup> which contained, respectively, 3 mol % N<sub>2</sub> and 5 mol % N<sub>2</sub>.

Table 3 also reports SLVE data available in the literature for the CO<sub>2</sub>–CH<sub>4</sub>–N<sub>2</sub> system: Riva and Stringari<sup>14</sup> examined two different mixtures containing, respectively, 2 mol % CO<sub>2</sub>, 58 mol % CH<sub>4</sub>, 40 mol % N<sub>2</sub> and 2 mol % CO<sub>2</sub>, 79 mol % CH<sub>4</sub>, 19 mol % N<sub>2</sub> and reported the measured composition of the liquid and vapor phases at each temperature and pressure. More details on these SLVE data are reported in Tables S19–S20 in the Supporting Information.

**2.3. The CO<sub>2</sub>–CH<sub>4</sub>–N<sub>2</sub>–O<sub>2</sub> system.** Riva and Stringari<sup>14</sup> reported some data concerning SLVE of the quaternary mixture comprising CO<sub>2</sub>, CH<sub>4</sub>, N<sub>2</sub>, and O<sub>2</sub> in order to better understand the influence of nitrogen and air content on phase equilibria. Table 4 summarizes the available data that, to our knowledge, are the only ones currently available for this system. More details on these experimental data are reported in Tables S21–S22 in the Supporting Information.

**Table 3. SVE and SLVE Experimental Data Available in the Literature for the CO<sub>2</sub>–CH<sub>4</sub>–N<sub>2</sub> System**

lit. source	measurement technique	data type	mixture	T [K]	P [bar]	no. points
SVE						
Haufe et al. (1972) <sup>20</sup>	sampling technique	frost points (T, P)	0.21 mol % CO <sub>2</sub> –36.5 mol % CH <sub>4</sub> –63.3 mol % N <sub>2</sub>	151.48 to 165.21	10.059 to 39.948	5 <sup>a</sup>
			0.45 mol % CO <sub>2</sub> –36.5 mol % CH <sub>4</sub> –63.0 mol % N <sub>2</sub>			
Agrawal and Laverman (1995) <sup>8</sup>	nonsampling visual technique	frost points (T, P)	0.96 mol % CO <sub>2</sub> –98.36 mol % CH <sub>4</sub> –0.68 mol % N <sub>2</sub>	154.15 to 172.76	1.724 to 24.407	19
			0.93 mol % CO <sub>2</sub> –96.13 mol % CH <sub>4</sub> –2.94 mol % N <sub>2</sub>			
Le and Trebble (2007) <sup>7</sup>	nonsampling visual technique	frost points (T, P)	1.94 mol % CO <sub>2</sub> –97.06 mol % CH <sub>4</sub> –1 mol % N <sub>2</sub>	173.90 to 183.50	12.437 to 22.615	24
			1.94 mol % CO <sub>2</sub> –96.11 mol % CH <sub>4</sub> –1.95 mol % N <sub>2</sub>			
Xiong et al. (2015) <sup>11</sup>	static analytic method with sampling technique	T–P–x <sub>V</sub>	CO <sub>2</sub> –CH <sub>4</sub> –3 mol % N <sub>2</sub> CO <sub>2</sub> –CH <sub>4</sub> –5 mol % N <sub>2</sub>	153.15 to 193.15	2.670 to 22.00	77
SLVE						
Riva and Stringari (2018) <sup>14</sup>	static analytic approach	T–P–x <sub>L</sub> –x <sub>V</sub>	2 mol % CO <sub>2</sub> –58 mol % CH <sub>4</sub> –40 mol % N <sub>2</sub> 2 mol % CO <sub>2</sub> –79 mol % CH <sub>4</sub> –19 mol % N <sub>2</sub>	124.5 to 145.9	5.2 to 20.4	6

<sup>a</sup>As reported by Agrawal and Laverman.<sup>8</sup>

**Table 4. SLVE Experimental Data Available in the Literature for the CO<sub>2</sub>–CH<sub>4</sub>–N<sub>2</sub>–O<sub>2</sub> System**

lit. source	data type	mixture composition	T [K]	P [bar]	no. points
Riva and Stringari (2018) <sup>14</sup>	T–P– x <sub>l</sub> – x <sub>v</sub>	2 mol % CO <sub>2</sub> –58 mol % CH <sub>4</sub> –31 mol % N <sub>2</sub> –9 mol % O <sub>2</sub>  2 mol % CO <sub>2</sub> –79 mol % CH <sub>4</sub> –15 mol % N <sub>2</sub> –4 mol % O <sub>2</sub>	125.1 to 146.5	5.8 to 21.1	6

### 3. ALGORITHM FOR THE SIMULTANEOUS COMPUTATION OF PHASE STABILITY AND MULTIPHASE EQUILIBRIA FOR SOLID, LIQUID, AND VAPOR PHASES

In this section, an algorithm for the simultaneous computation of phase stability and multiphase equilibria of CO<sub>2</sub> mixtures with hydrocarbons and nonhydrocarbon components is presented. The proposed algorithm overcomes one of the common problems encountered in the calculation of phase equilibria (e.g., when based on the isofugacity condition),<sup>21</sup> that is, that the number of phases which are present at equilibrium are not known *a-priori*. The adopted stability criterion was first presented in the literature by Gupta<sup>22</sup> as an alternative to other approaches (e.g., those proposed by Gautam and Seider,<sup>23</sup> Michelsen,<sup>24–26</sup> Wu and Bishnoi,<sup>27</sup> Castier et al.<sup>28</sup>). Gupta and coauthors applied such a method to systems for which vapor–liquid–liquid equilibrium (VLE) conditions can be established, such as the ethanol–ethyl acetate–water system<sup>29</sup> and the CO<sub>2</sub>–CH<sub>4</sub>–H<sub>2</sub>S system.<sup>30</sup> This stability criterion was later applied by Ballard and Sloan<sup>31</sup> and by Segtovich et al.<sup>32</sup> to systems involving several phases of interest (including gas hydrates) in order to perform multiphase flashes. More recently, Tang and co-workers<sup>33</sup> have extended the algorithm developed by Gupta<sup>22</sup> to compute SVE, SLE, and SLVE of the CO<sub>2</sub>–CH<sub>4</sub> mixture. In their study, the fugacity coefficients of fluid phases (i.e., vapor and liquid) were calculated using GERG-2004 multiparameter equation of state (EoS), while the EoS that described the thermodynamic behavior of solid CO<sub>2</sub> was based on the Gibbs free energy method suggested by Jäger and Span.<sup>34</sup>

In this work, the approach proposed by Gupta<sup>22</sup> has been implemented in a Fortran code to couple phase stability and isothermal–isobaric flash calculations that involve the vapor, liquid, and/or solid phases, with the latter one assumed to consist of pure CO<sub>2</sub>. To our knowledge, this approach has never been applied to phase equilibria involving solid CO<sub>2</sub> for multicomponent systems, and the difference with respect to previous literature works,<sup>33</sup> focused on the CO<sub>2</sub>–CH<sub>4</sub> binary system only, lies in the different thermodynamic models used for the properties of fluid phases and of solid CO<sub>2</sub>. Indeed, in this work, the Peng–Robinson EoS has been used for computing the fugacities of the fluid phases, whereas the fugacity of pure CO<sub>2</sub> in the solid phase has been expressed by relating it to the fugacity of pure CO<sub>2</sub> in the vapor phase, without any derivation from a hypothetical subcooled liquid fugacity. The implementation for multicomponent systems, of which the novelty of this work consists, finds practical application in the study and correct design of many CO<sub>2</sub> removal processes operated at low-temperature/cryogenic conditions. For example, the proposed algorithm can be used to check if a mixture of interest will form solid CO<sub>2</sub> at certain temperature and pressure conditions, such as those at some

trays of low-temperature distillation columns that have been recently studied for the sweetening of high CO<sub>2</sub>-content natural gases<sup>35</sup> or for the upgrading of biogas.<sup>36</sup> Indeed, commercial simulation software often does not take into account the formation of CO<sub>2</sub>(s). This is one of the possible applications of the proposed algorithm, which helps determine the operating conditions that ensure the correct operation of processes.

The theoretical background for the algorithm implemented in this work is outlined in the [Supporting Information](#), for the sake of clarity. In the following, the implementation of the algorithm is discussed, which requires the following input data, as illustrated in [Figure 1](#): temperature *T*, pressure *P*, and the global composition (*z<sub>i</sub>* refers to the mole fraction of the *i*th component in the feed stream).

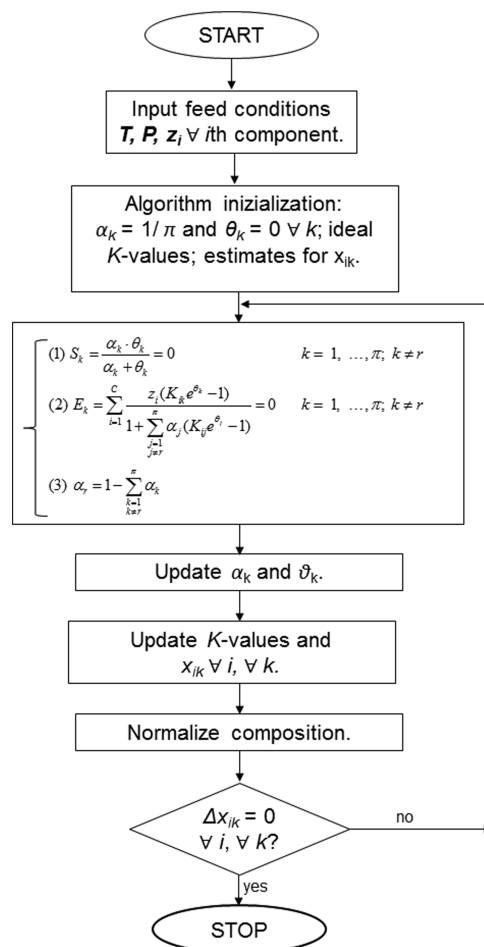


**Figure 1.** Block diagram of the proposed algorithm that simultaneously performs isothermal–isobaric flash calculations and a phase stability analysis.

The algorithm is started assuming all phases are present with an equal amount of each, and, therefore, their stability variables ( $\theta_k$ ) are all zero.<sup>37</sup> The initialization of the Gibbs energy minimization algorithm also requires a set of *K*-values that are composition-independent (also commonly referred to as ideal *K*-values). The initial estimate for the mole fraction of each component ( $i = 1, \dots, C$ ) in each phase ( $k = 1, \dots, \pi$ ) has been computed according to eq S14 in the [Supporting Information](#), in which the implemented algorithm takes into account the



molar phase fraction  $\alpha_k = 1/\pi$  and the stability variable  $\theta_k = 0$  for all  $k$  phases ( $k = 1, \dots, \pi$ ).

Then, the first part of the problem to be solved, which can be referred to as “inner loop”, consists in minimizing the Gibbs free energy of the system at a given set of  $K$ -values and composition. The following system of  $(2\pi - 1)$  equations is solved in the  $(2\pi - 1)$  unknowns,  $\alpha_k$  ( $k = 1, \dots, \pi$ ) and  $\theta_k$  ( $k = 1, \dots, \pi$  and  $k \neq r$ ).

$$\begin{cases} S_k = \frac{\alpha_k \cdot \theta_k}{\alpha_k + \theta_k} = 0 & \text{for } k = 1, \dots, \pi \text{ and } k \neq r \\ E_k = \sum_{i=1}^C \frac{z_i(K_{ik}e^{\theta_k} - 1)}{1 + \sum_{j=1, j \neq r}^{\pi} \alpha_j(K_{ij}e^{\theta_j} - 1)} = 0 & \text{for } k = 1, \dots, \pi \text{ and } k \neq r \\ \alpha_r = 1 - \sum_{\substack{k=1 \\ k \neq r}}^{\pi} \alpha_k \end{cases} \quad (1)$$

The Newton procedure is used to solve the above system, which requires expressing the derivatives of the equations above with respect to each unknown variable. To avoid incurring a singular Jacobian during the iterations, the technique presented by Gupta et al.<sup>30</sup> has been implemented. It consists in selecting a small positive number,  $\varepsilon$ , set equal to  $1 \times 10^{-10}$ , so that whenever  $\alpha_k$  becomes less or equal to  $\varepsilon$  while  $\theta_k$  is zero, both  $\alpha_k$  and  $\theta_k$  are set equal to  $\varepsilon$ . The same occurs whenever  $\theta_k$  becomes less or equal to  $\varepsilon$  while  $\alpha_k$  is zero. For the special case in which both  $\alpha_k$  and  $\theta_k$  are less than  $\varepsilon$ , the solution of the system remains at the point  $\alpha_k = \theta_k = \varepsilon$ .

After the inner loop is solved and the values for  $\alpha_k$  and  $\theta_k$  are updated, it is then possible to calculate in the outer loop the mole fraction of each component ( $i = 1, \dots, C$ ) in each phase ( $k = 1, \dots, \pi$ ), using eq S14 reported in the [Supporting Information](#). From this point on, the  $K$ -values are calculated removing the assumption according to which they were assumed composition-independent.

Recalling the definition of the  $K$ -values as the ratios of fugacity coefficients of component  $i$  between phase  $k$  and the reference phase  $r$ , it is necessary to define  $K$ -values that correspond to some reference phase. Their expressions are reported in [Table 5](#), depending on which phase is taken as the reference one. As previously reported, the fugacity coefficients in the vapor and liquid phases have been calculated with the Peng–Robinson EoS.<sup>38</sup> On the contrary, the fugacity of pure solid CO<sub>2</sub> has been expressed using a model different from the one suggested by Jäger and Span<sup>34</sup> and by relating it to the one in the vapor phase, which requires computing its solid vapor pressure ( $P_{\text{subl},i}$  for  $i = \text{CO}_2$  in [Table 5](#)) at the system temperature and the fugacity coefficient of CO<sub>2</sub> in the vapor phase at the system temperature and pressure, if the Poynting correction term is neglected. The dependence of the solid vapor pressure upon temperature can be expressed according to the six-parameter correlation proposed by Jensen et al.,<sup>39</sup> which has been used in this work.

Calculations are performed until convergence is reached in the outer loop on the normalized composition of all phases. If convergence is not reached using a reference phase (the vapor phase is tried first), the calculation is repeated taking the liquid and, if needed, the solid phase as the reference one.

In this work, two types of phase equilibrium problems are investigated concerning SVE and SLVE conditions.

When SVE conditions are given in the literature in terms of CO<sub>2</sub> frost points as  $T$ ,  $P$  pairs, the calculation has been carried

**Table 5. Expressions for Composition-Dependent  $K_{ik}$  Assuming Different Phases as the Reference ( $r$ ) Phase**

$K_{ik}$	$r = V$	$r = L$	$r = S$
$K_{iV}$	$= \frac{x_{iL}}{x_{iV}} = 1$	$= \frac{x_{iV}}{x_{iL}} = \frac{\hat{\phi}_i^L(T, P, \mathbf{x}_L)}{\hat{\phi}_i^V(T, P, \mathbf{x}_V)}$	$= \frac{x_{iV}}{x_{iS}} \rightarrow \infty$ , for $i \neq \text{CO}_2$ $= \frac{x_{iV}}{x_{iS}} = \frac{P_{\text{subl},i}(T) \cdot \hat{\phi}_i^V(T, P, \mathbf{x}_V)}{P \cdot \hat{\phi}_i^V(T, P, \mathbf{x}_V)}$ , for $i = \text{CO}_2$
$K_{iL}$	$= \frac{x_{iL}}{x_{iV}} = \frac{\hat{\phi}_i^V(T, P, \mathbf{x}_V)}{\hat{\phi}_i^L(T, P, \mathbf{x}_L)}$	$= \frac{x_{iL}}{x_{iL}} = 1$	$= \frac{x_{iL}}{x_{iS}} \rightarrow \infty$ , for $i \neq \text{CO}_2$ $= \frac{x_{iL}}{x_{iS}} = \frac{P_{\text{subl},i}(T) \cdot \hat{\phi}_i^V(T, P, \mathbf{x}_V)}{P \cdot \hat{\phi}_i^L(T, P, \mathbf{x}_L)}$ , for $i = \text{CO}_2$
$K_{iS}$	$\left. \begin{aligned} & (0, \text{ for } i \neq \text{CO}_2) \\ & = \frac{x_{iS}}{x_{iV}} = \frac{P \cdot \hat{\phi}_i^V(T, P, \mathbf{x}_V)}{P_{\text{subl},i}(T) \cdot \hat{\phi}_i^V(T, P, \mathbf{x}_V)} \end{aligned} \right\}$ , for $i = \text{CO}_2$	$\left. \begin{aligned} & (0, \text{ for } i \neq \text{CO}_2) \\ & = \frac{x_{iS}}{x_{iL}} = \frac{P \cdot \hat{\phi}_i^L(T, P, \mathbf{x}_L)}{P_{\text{subl},i}(T) \cdot \hat{\phi}_i^V(T, P, \mathbf{x}_V)} \end{aligned} \right\}$ , for $i = \text{CO}_2$	$= \frac{x_{iS}}{x_{iS}} = 1$

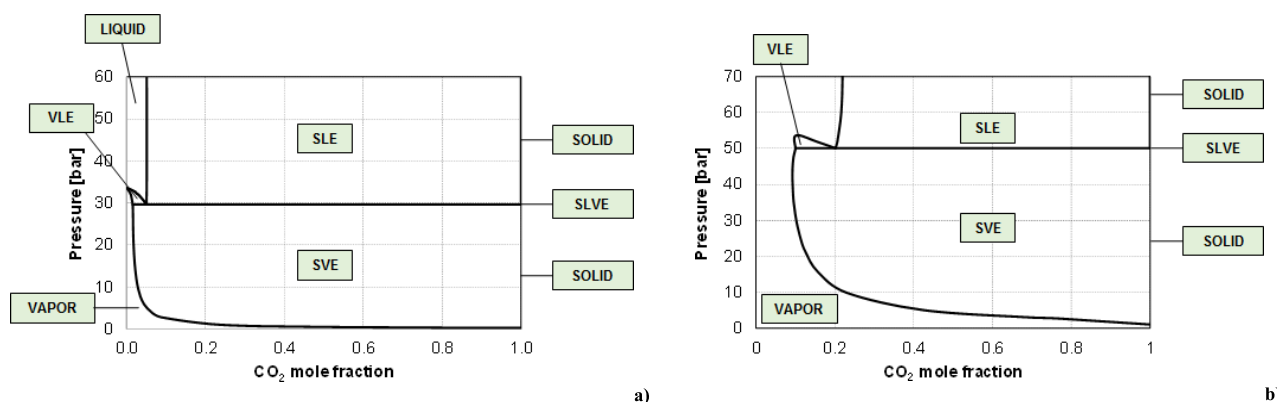


**Figure 2.** Pressure–composition diagram constructed using the proposed algorithm for the  $\text{CO}_2$ – $\text{CH}_4$  binary mixture at (a) 178.15 K; (b) 203.15 K.

out at the same global composition (typically available) and pressure as the experimental ones, whereas the temperature has been varied so that the highest value for which the  $\text{CO}_2$  solidification ratio (corresponding to the ratio  $\alpha_S/z_{\text{CO}_2}$ ) is greater than or equal to 0.0001 is considered as the temperature of the frost point. Such a calculated temperature is compared with the experimental one reported in the literature.

Considering the data sets reporting SVE measurements as  $P-x_{\text{CO}_2,V}$  at a given temperature, these do not always include the global composition of the mixture charged into the equilibrium cell. This is the case, for example, for some data available in the literature for the  $\text{CO}_2$ – $\text{CH}_4$  binary mixture.<sup>6,11</sup> Therefore, to provide the required input data to the Fortran code, it has been necessary to assume a global composition for the system. To do that, the behavior of the  $\text{CO}_2$ – $\text{CH}_4$  binary system has been taken into account, which is shown, for the sake of clarity, in the  $P$ -composition diagrams in Figure 2 for the two temperatures of 178.15 K and 203.15 K (respectively, lower and higher than the critical temperature of methane, i.e., 190.6 K<sup>40</sup>). These two diagrams have been constructed by running the Fortran code several times with different input data. Since the temperature is fixed (at, respectively, 178.15 K and 203.15 K in Figure 2a and in Figure 2b), the overall composition has been assigned (starting, for example, from an equimolar mixture of the two components) and the isothermal–isobaric flash has been solved for different input values of the pressure (read from an array), obtaining the phases present at equilibrium and their composition, which is plotted in Figure 2. The same procedure has been followed by changing the input global composition so that all types of equilibria (e.g., also the small VLE region) could be shown. The two diagrams in Figure 2 are qualitatively representative of the same diagrams at temperatures, respectively, lower and higher than the critical temperature of methane. Therefore, based on this behavior, when considering the data sets reporting SVE measurements as  $P-x_{\text{CO}_2,V}$  at a given temperature, the global composition has been assigned setting the  $\text{CO}_2$  mole fraction at a value higher than the mole fraction in the vapor phase at equilibrium as determined experimentally.

For the ternary mixture, the SVE data collected by Xiong and co-workers<sup>11</sup> are given in terms of temperature, pressure, composition of the vapor phase at equilibrium and a given mole fraction of  $\text{N}_2$  in the ternary mixture (i.e., 3 mol % or 5 mol %). In this case, the global composition has been assigned

considering the given mole fraction of  $\text{N}_2$  and a mole fraction of  $\text{CO}_2$  greater than the one in the vapor phase at equilibrium.

To use the proposed algorithm for SLVE calculations for the  $\text{CO}_2$ – $\text{CH}_4$  binary mixture and for ternary and quaternary mixtures also containing  $\text{N}_2$  and  $\text{O}_2$ , this procedure has been followed. As for the binary mixture, a global composition has been assumed and, at a given temperature set equal to the available experimental value, the SLVE pressure has been determined. In fact, for the binary mixture, at a fixed temperature, SLVE conditions are established at a unique pressure. This is not the case if the pressure were fixed instead, due to the maximum shape of the SLVE locus for the  $\text{CO}_2$ – $\text{CH}_4$  mixture (as shown in the following in Figure 7), which implies that for certain pressures there exist two temperatures at which dry ice can coexist with the vapor and liquid phases.

In the case of mixtures also containing nitrogen and/or oxygen, when the global composition, the temperature, and the pressure are reported in the literature,<sup>14</sup> all the input data required by the proposed algorithm are available. Therefore, it is possible to use it to calculate the composition of the phases present at equilibrium and make a comparison with that available in the literature.

The results are reported in the following together with those that can be obtained using the RIGbbs tool<sup>41</sup> available in Aspen Plus V9.0.<sup>42</sup> To our knowledge, it is the only tool that is able to deal with this type of phase equilibria: it uses Gibbs energy minimization techniques to compute equilibrium instead of methods based on the equality of the fugacity of each component in each phase. The system is considered at equilibrium when the distribution of the components of a system is obtained such that the Gibbs energy is minimal (subject to atom balance constraints). According to the literature from Aspen Technology, the method based on Gibbs energy minimization can be used for any number of phases and components and always yields stable solutions. To be consistent with the models of which our algorithm makes use, we have selected the Peng–Robinson EoS, which applies to fluid phases. To calculate enthalpies, entropies, and Gibbs free energies for conventional components in the vapor and/or liquid phase, the simulator uses the standard heat of formation and standard Gibbs free energy of formation. On the contrary, the standard solid heat of formation and standard solid Gibbs free energy of formation for the component of “solid” type (i.e., solid  $\text{CO}_2$ ) present in our simulation need to be specified. Then, other properties (for which the default options have

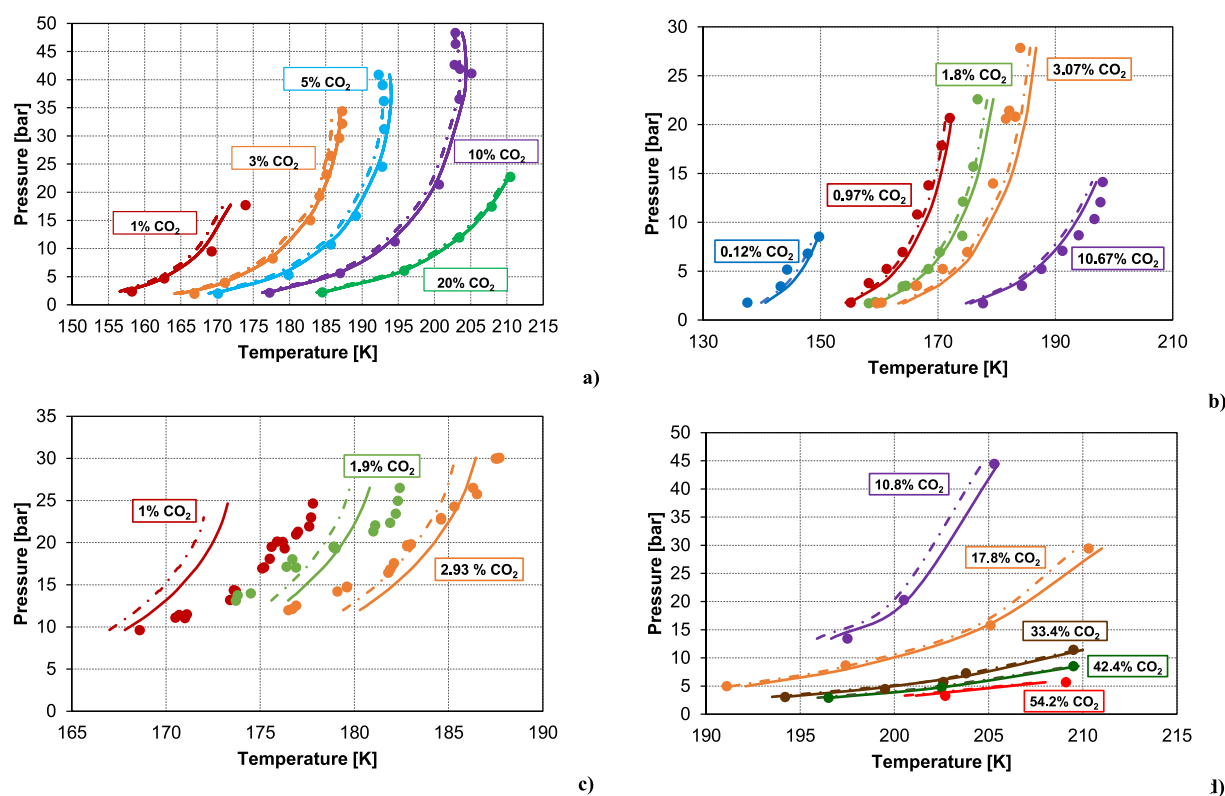


**Figure 3.** Comparison between the results obtained with the proposed algorithm (solid line), by simulation with RGibbs in Aspen Plus V9.0<sup>42</sup> (dashed and dotted line), and the experimental data of frost points for the CO<sub>2</sub>-CH<sub>4</sub> mixture for different data sets: (a) Pikaar;<sup>6</sup> (b) Agrawal and Laverman;<sup>8</sup> (c) Le and Trebble;<sup>7</sup> (d) Zhang et al.<sup>9</sup>

been kept) are used by the simulator to calculate each property at a given temperature and pressure.

#### 4. RESULTS AND DISCUSSION

In this section, the results obtained with the proposed algorithm are discussed taking into account the average absolute deviation (AAD%) calculated according to the generic equation:

$$\text{AAD}\% = \frac{100}{n} \sum_{i=1}^n \frac{|\nu_{\text{calc},i} - \nu_{\text{exp},i}|}{\nu_{\text{exp},i}} \quad (2)$$

where  $\nu_{\text{calc}}$  refers to the calculated value of the generic variable (e.g., the temperature in the case of CO<sub>2</sub> frost point calculations),  $\nu_{\text{exp}}$  refers to the experimental value of the same generic variable, and  $n$  stands for the number of experimental available data.

In the following, the results for the CO<sub>2</sub>-CH<sub>4</sub> binary mixture are illustrated first (section 4.1). Then, in sections 4.2 and 4.3, the results obtained for mixtures also containing nitrogen and oxygen are shown.

The experimental data are reported with the corresponding error bar, when this information was available in the literature.

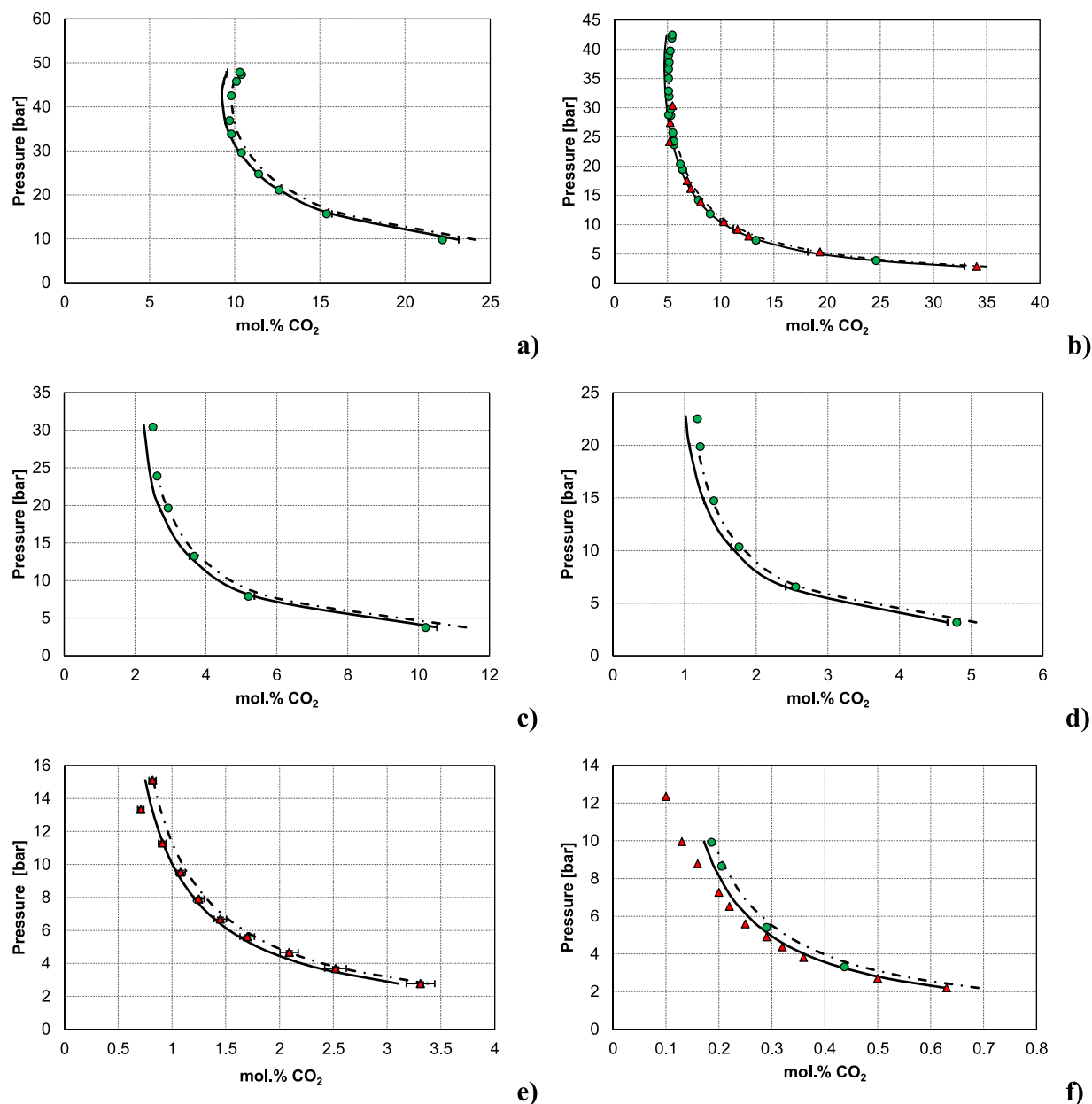
**4.1. The CO<sub>2</sub>-CH<sub>4</sub> System.** Results for the calculation of frost point temperatures are illustrated in Figure 3. The AAD% for each literature source is reported in Table 6.

Figure 4 shows the results for SVE calculations on  $P$ -composition diagrams. It is possible to observe that there exists a good agreement between the two different approaches and the experimental data, with an overall AAD% equal to 5.86% for the proposed algorithm and 5.04% for the RGibbs tool when considering the data set by Pikaar<sup>6</sup> and, respectively,

**Table 6.** AAD% (eq 2) in the Calculation of Frost Points for the CO<sub>2</sub>-CH<sub>4</sub> System

lit. source	this work	RGibbs
Pikaar (1959) <sup>6</sup>	0.360	0.574
Agrawal and Laverman (1995) <sup>8</sup>	1.079	0.873
Le and Trebble (2007) <sup>7</sup>	1.239	1.364
Zhang et al. (2011) <sup>9</sup>	0.297	0.375

7.61% and 8.34% when considering the data set by Xiong et al.<sup>11</sup> In particular, higher deviations are observed at low concentrations, as illustrated in Figure 5, which presents percentage differences between CO<sub>2</sub>  $K$ -values from calculations and data plotted against the mole percentage of CO<sub>2</sub> in the vapor phase. Indeed, when considering the proposed approach the calculated  $K$ -values agree with the experimental data to within  $\pm 14\%$  at high concentrations and temperatures (203.15 K to 173.15 K, Figure 5a-d), whereas they agree to within  $\pm 32\%$  at low concentrations and temperatures (168.15 K and 153.15 K in Figure 5e,f). This may be also due to greater uncertainties of the experimental data at these conditions. It is also interesting to notice that larger deviations are observed, considering the same composition range and temperature, for the data by Xiong et al.<sup>11</sup> (Figure 5b and Figure 5f). Indeed, at the lowest CO<sub>2</sub> concentrations and temperature (Figure 5f), the  $K$ -values calculated with the proposed approach are underestimated by maximum 7.5% with the experimental data by Pikaar<sup>6</sup> only (i.e., by neglecting the data by Xiong et al.<sup>11</sup>). These differences may be explained considering that the experimental procedure used in the two works is different, as well as the analysis technique. Pikaar<sup>6</sup> used a saturation cell apparatus, the walls of which were coated at the beginning with



**Figure 4.** Comparison between the results obtained with the proposed algorithm (solid line) and by simulation with RGibbs in Aspen Plus V9.0<sup>42</sup> (dashed and dotted line), and the experimental SVE data for the CO<sub>2</sub>–CH<sub>4</sub> system (green dots, data by Pikaar,<sup>6</sup> red triangles, data by Xiong et al.<sup>11</sup>) at different temperatures: (a) 203.15 K; (b) 193.15 K; (c) 183.15 K; (d) 173.15 K; (e) 168.15 K; (f) 153.15 K.

solid CO<sub>2</sub> and in which some methane was fed, after cooling to the cryostat temperature; then, the saturated methane left the cell, was warmed to room temperature outside the bath and expanded to atmospheric pressure; the samples were analyzed by infrared absorption. Xiong et al.<sup>11</sup> performed their measurements by first filling the equilibrium cell with the test gas mixture as to guarantee the CO<sub>2</sub> content in it to be slightly higher than the predicted content at frost point. Then, they filled the constant temperature bath with helium and the container with liquid nitrogen, set the temperature and waited for equilibrium to be reached, sampled the gas mixture, and analyzed its composition by a gas chromatograph.

Moreover, since the agreement between calculated results and experimental data in Figure 4 is less satisfactory at higher pressures, we investigated the effect due to the Poynting correction factor that has not been taken into account in the

expression of  $K_{iS}$  in Table 5. If that expression is modified as in eqs 3 to 4, where the solid molar volume ( $v_S$ ) has been taken from the literature,<sup>41</sup> then the AAD% for the proposed algorithm decreases to 3.74% and 7.47%, respectively, for the two data sets presented by Pikaar<sup>6</sup> and Xiong et al.,<sup>11</sup> allowing acquisition of better performances, in particular for the data set presented by Pikaar.<sup>6</sup>

$$K_{iS}(r = V) = \begin{cases} 0, & \text{for } i \neq \text{CO}_2 \\ \frac{x_{iS}}{x_{iV}} = \frac{P \cdot \phi_i^V(T, P, \mathbf{x}_V)}{P_{\text{subl},i}(T) \cdot \phi_i^V(T, P_{\text{subl},i}(T)) \exp\left[\frac{v_{iS}(P - P_{\text{subl},i}(T))}{RT}\right]}, & \text{for } i = \text{CO}_2 \end{cases} \quad (3)$$



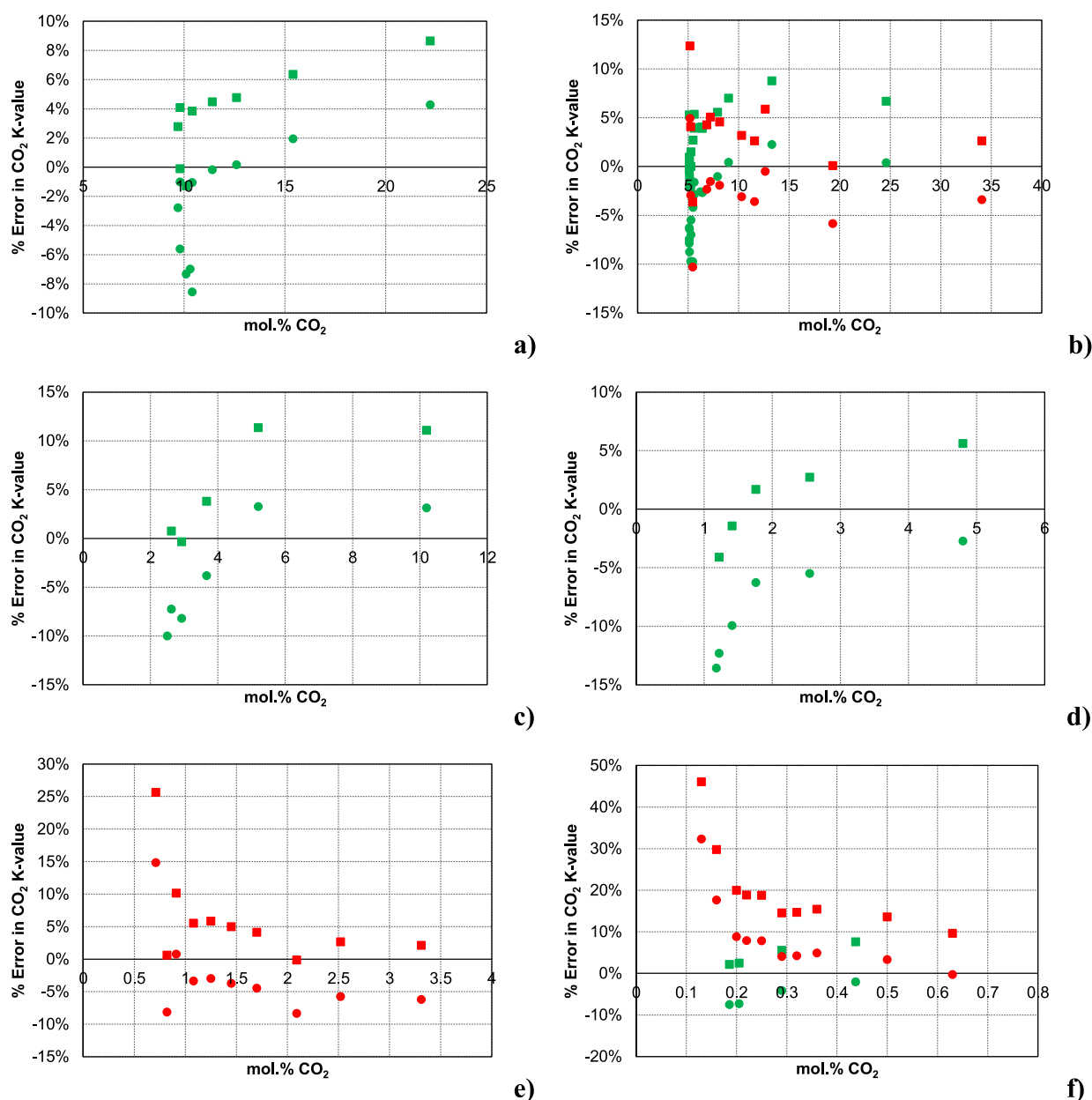


**Figure 5.** Percentage errors of  $K$ -value of CO<sub>2</sub> obtained with the proposed algorithm (●) and by simulation of RGibbs in Aspen Plus V9.0<sup>42</sup> (■) in comparison to the SVE experimental data by Pikaar<sup>6</sup> (green) and by Xiong et al.<sup>11</sup> (red) at different temperatures: (a) 203.15 K; (b) 193.15 K; (c) 183.15 K; (d) 173.15 K; (e) 168.15 K; (f) 153.15 K.

$$K_{iS}(r=L) = \begin{cases} 0, & \text{for } i \neq \text{CO}_2 \\ \frac{x_{iS}}{x_{iL}} = \frac{P \hat{\phi}_i^L(T, P, \mathbf{x}_L)}{P_{\text{subl},i}(T) \cdot \phi_i^V(T, P_{\text{subl},i}(T)) \exp\left[\frac{v_i(P - P_{\text{subl},i}(T))}{RT}\right]}, & \text{for } i = \text{CO}_2 \end{cases} \quad (4)$$

Focusing the attention on Figure 3c, it is possible to observe that the results obtained with both approaches differ from the experimental data provided by Le and Trebble.<sup>7</sup> To achieve a better understanding of this, experimental frost point data from different literature sources at similar global composition have been compared, as shown in Figure 6.

As can be noticed from Figure 6, at higher pressures and lower amounts of carbon dioxide in the initial mixture, where the largest disagreement exists, the data collected by Le and

Treble<sup>7</sup> lie more closely to the data collected by Pikaar<sup>6</sup> and both are shifted to the right with respect to the data of Agrawal and Laverman.<sup>8</sup> However, the experimental data reported by Pikaar<sup>6</sup> cover a lower pressure range (from 2 to 18 bar) with respect to the ones presented by Le and Trebble<sup>7</sup> (from 9 to 25 bar), with only two points from Pikaar<sup>6</sup> in the same pressure range. Therefore, it is not possible to state if some of the data sets available in the literature are not reliable. On the contrary, at higher amounts of carbon dioxide (Figure 6c,d) the experimental data reported by the different authors are very close to each other.

As for the SLVE locus for the CO<sub>2</sub>–CH<sub>4</sub> system, results are shown in Figure 7. The results obtained with the proposed algorithm (solid line) are in good agreement with the experimental data, except for those by Donnelly and Katz,<sup>15</sup> which however deviate from the other experimental data.

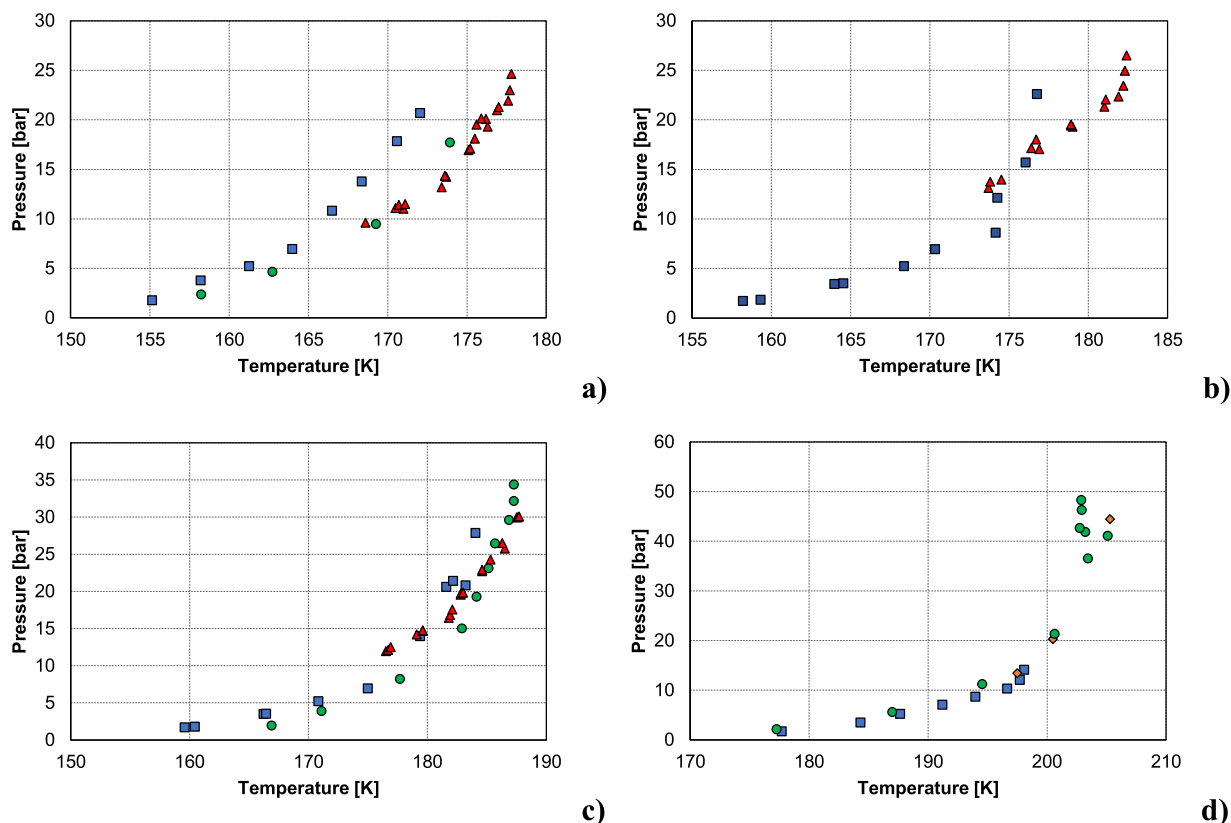


**Figure 6.** Comparison of the experimental frost point data for the  $\text{CO}_2\text{-CH}_4$  system by Pikaar<sup>6</sup> (green dots), Agrawal and Laverman<sup>8</sup> (blue squares), Le and Trebble<sup>7</sup> (red triangles), and Zhang et al.<sup>9</sup> (orange diamonds) for four different global compositions: (a) around 1 mol %  $\text{CO}_2$ ; (b) around 2 mol %  $\text{CO}_2$ ; (c) around 3 mol %  $\text{CO}_2$ ; (d) around 10 mol %  $\text{CO}_2$ .

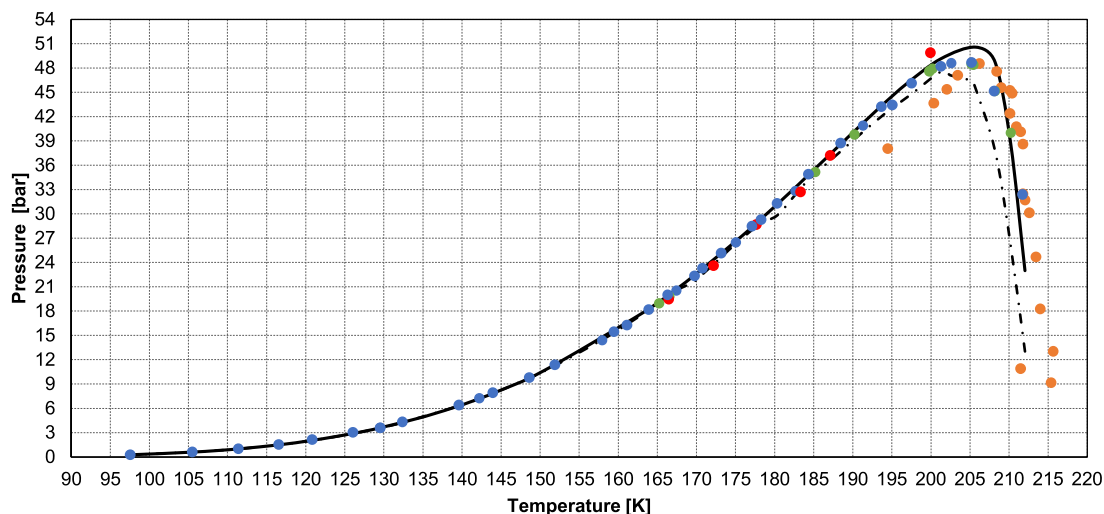


**Figure 7.** SLVE pressure as a function of temperature: comparison between the results obtained with the proposed algorithm (solid line), with the RGibbs tool of Aspen Plus V9.0<sup>42</sup> (dashed and dotted line), and the experimental data available in the literature. The different colors refer to different works: orange, Donnelly and Katz;<sup>15</sup> red, Sterner;<sup>16</sup> light blue, Davis et al.;<sup>17</sup> green, Im and Kurata.<sup>18</sup>

Indeed, the locus of triple points by Donnelly and Katz<sup>15</sup> results to be lower in pressure or, conversely, higher in temperature than the results obtained with the proposed algorithm. As for the two calculation approaches, some differences are observed at higher temperature values (i.e., above 195 K), where the SLVE locus obtained using the RGibbs tool lies below the locus obtained using the proposed algorithm. The AAD% for the proposed algorithm and the

RGibbs tool are, respectively, 4.27% and 8.94% if all the available data are considered, whereas lower values are obtained (respectively, 2.20% and 4.81% for the two approaches) if the data from Donnelly and Katz<sup>15</sup> are not taken into account. Figure 8 shows the results for each experimental data set. Since the Peng–Robinson EoS<sup>38</sup> has been used as the thermodynamic model for the fluid phases both in the proposed algorithm and in the setup of the

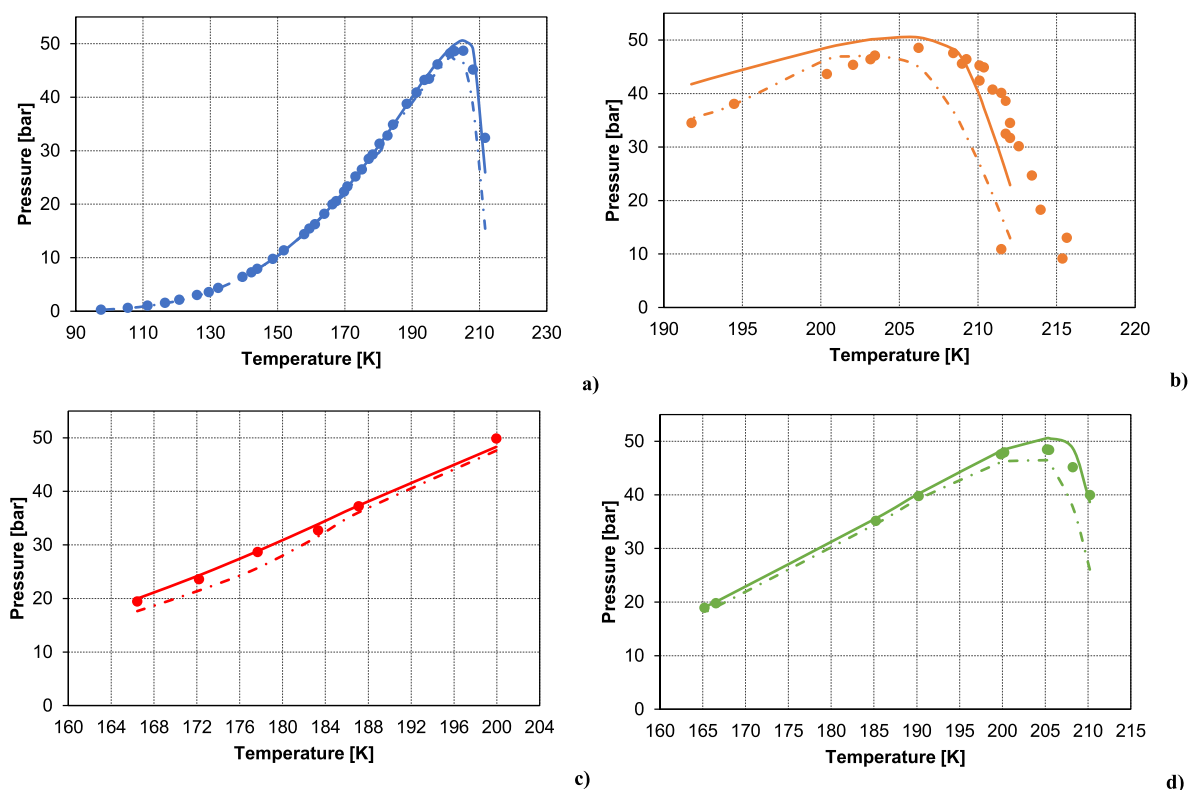


**Figure 8.** SLVE pressure as a function of temperature: comparison between the results obtained with the proposed algorithm (solid line), with the RGibbs tool of Aspen Plus V9.0<sup>42</sup> (dashed and dotted line), and the experimental data reported by (a) Davis et al.;<sup>17</sup> (b) Donnelly and Katz;<sup>15</sup> (c) Sterner;<sup>16</sup> (d) Im and Kurata.<sup>18</sup>

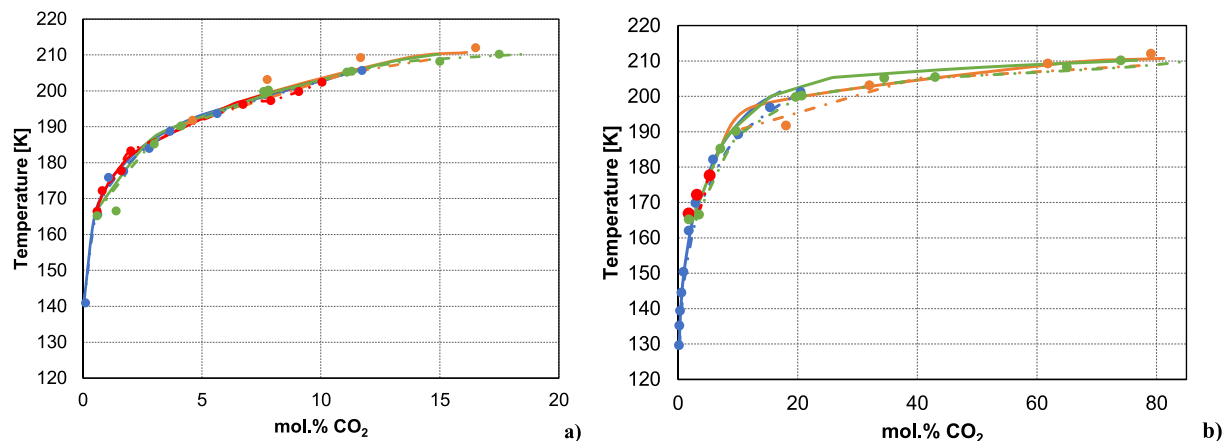


**Figure 9.** Mole percentage of CO<sub>2</sub> as a function of temperature in (a) vapor phase at SLVE; (b) liquid phase at SLVE. Comparison between the results obtained with the proposed algorithm (solid lines), by using the RGibbs tool of Aspen Plus V9.0<sup>42</sup> (dashed and dotted line), and experimental data. The different colors refer to different literature sources: orange, Donnelly and Katz;<sup>15</sup> red, Sterner;<sup>16</sup> light blue, Davis et al.;<sup>17</sup> green, Im and Kurata.<sup>18</sup>

simulation in Aspen Plus using the RGibbs tool, the differences observed in the results obtained with the two approaches can be explained considering that they are based on different models for calculating the fugacity and the properties of the solid phase (i.e., pure solid CO<sub>2</sub>).

Calculations have been also performed for the equilibrium composition of the vapor and liquid phases as a function of temperature, and the results are illustrated in Figure 9. For the data for which only the temperature and mole fraction of CO<sub>2</sub> were available in the literature, the pressure has been set equal to the value obtained by using each calculation method.

Calculation results are in good agreement with the experimental data, to a greater extent for the composition of the vapor phase.

**4.2. The CO<sub>2</sub>–CH<sub>4</sub>–N<sub>2</sub> System.** Results for frost point calculations for the CO<sub>2</sub>–CH<sub>4</sub>–N<sub>2</sub> ternary system are illustrated in Figure 10 and in Figure 11 considering the data sets presented, respectively, by Agrawal and Laverman<sup>8</sup> and by Le and Trebble.<sup>7</sup> Focusing on Figure 10, it is possible to observe that both approaches and, in particular, the proposed one, are conservative in the prediction of the CO<sub>2</sub> frost point temperature. If Figure 11 is taken into account, it is possible to

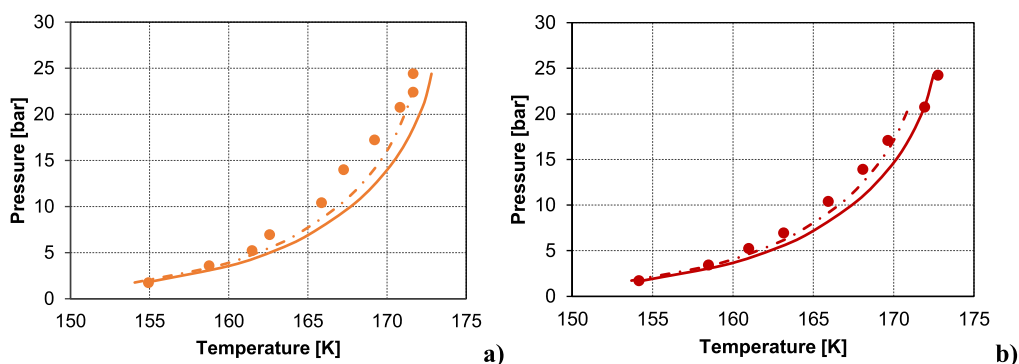


**Figure 10.** Comparison between the results obtained with the proposed algorithm (solid line), by simulation with RGibbs in Aspen Plus V9.0<sup>42</sup> (dashed and dotted line), and the experimental frost point data for the CO<sub>2</sub>–CH<sub>4</sub>–N<sub>2</sub> system by Agrawal and Laverman<sup>8</sup> for two different CO<sub>2</sub>–CH<sub>4</sub>–N<sub>2</sub> mixtures: (a) 0.96 mol % CO<sub>2</sub>, 98.36 mol % CH<sub>4</sub>, 0.68 mol % N<sub>2</sub>; (b) 0.93 mol % CO<sub>2</sub>, 96.13 mol % CH<sub>4</sub>, 2.94 mol % N<sub>2</sub>.

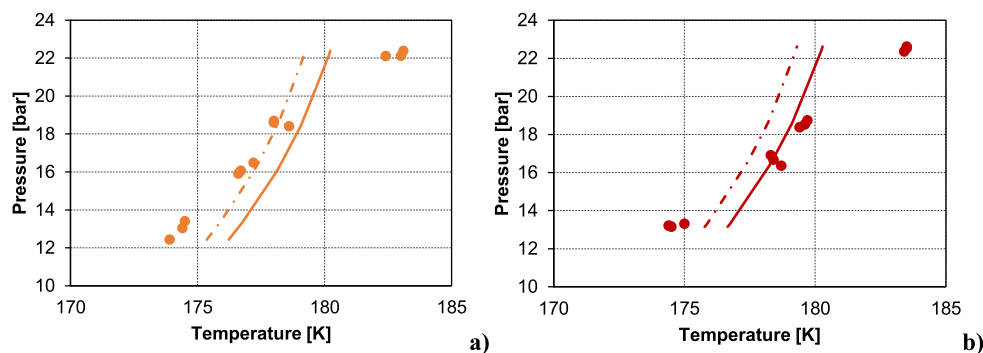


**Figure 11.** Comparison between the results obtained with the proposed algorithm (solid line), by simulation with RGibbs in Aspen Plus V9.0<sup>42</sup> (dashed and dotted line), and the experimental frost point data for the CO<sub>2</sub>–CH<sub>4</sub>–N<sub>2</sub> system by Le and Trebble<sup>7</sup> for two different CO<sub>2</sub>–CH<sub>4</sub>–N<sub>2</sub> mixtures: (a) 1.94 mol % CO<sub>2</sub>, 97.06 mol % CH<sub>4</sub>, 1 mol % N<sub>2</sub>; (b) 1.94 mol % CO<sub>2</sub>, 96.11 mol % CH<sub>4</sub>, 1.95 mol % N<sub>2</sub>.

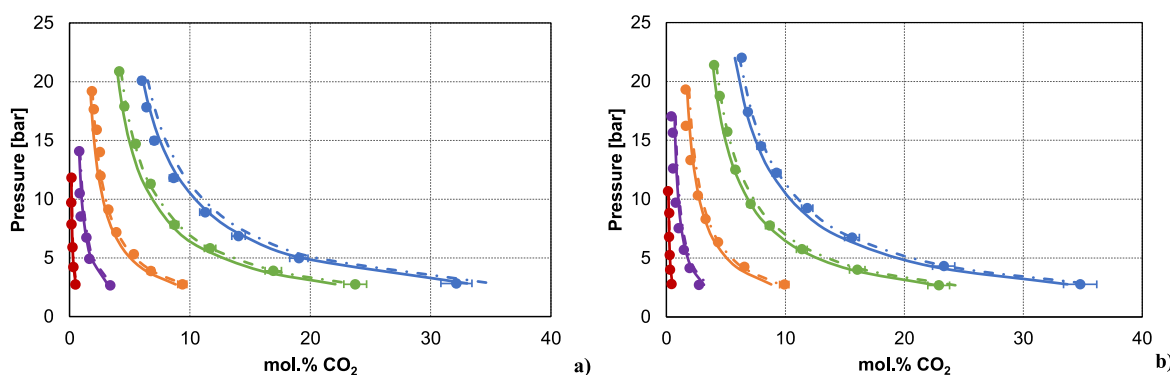


**Figure 12.** Comparison between the results obtained with the proposed algorithm (solid line), by simulation of RGibbs in Aspen Plus V9.0<sup>42</sup> (dashed and dotted line) and the SVE experimental data by Xiong et al.<sup>11</sup> for the (a) CO<sub>2</sub>–CH<sub>4</sub>–3 mol % N<sub>2</sub> mixture; (b) CO<sub>2</sub>–CH<sub>4</sub>–5 mol % N<sub>2</sub> mixture. The different colors refer to five different temperatures: 193.15 K (light blue); 188.15 K (green); 178.15 K (orange); 168.15 K (purple); 153.15 K (red).

observe that the results obtained with both approaches deviate from the experimental data provided by Le and Trebble,<sup>7</sup> but the overall AAD% is still acceptable (0.91% and 0.94%, respectively, for the proposed algorithm and the RGibbs tool).

The results of the calculations performed for the SVE data reported by Xiong et al.<sup>11</sup> are shown in Figure 12 for the five given temperatures and the two mixtures containing, respectively, 3 mol % (Figure 12a) and 5 mol % N<sub>2</sub> (Figure 12b). The results from calculations agree with the experimental data and confirm the experimental evidence according to which with the increase of the nitrogen content, the maximum pressure for CO<sub>2</sub> desublimation increases as well.<sup>11</sup>

The SLVE for the CO<sub>2</sub>–CH<sub>4</sub>–N<sub>2</sub> system was investigated by Riva and Stringari,<sup>14</sup> who presented experimental data for two mixtures as well as the results of their calculation approach. Such an approach is based on the isofugacity of the solid former component (i.e., CO<sub>2</sub>) in the liquid, vapor, and solid phases, which can be assumed as pure CO<sub>2</sub>, and makes use of the GERG 2008 multiparameter EoS for computing the fugacity in the fluid phases, while the fugacity of the solid phase was calculated using the model reported by Jäger and Span.<sup>34</sup> Figures 13 and 14 compare the results obtained with the proposed algorithm with those obtained by Riva and Stringari,<sup>14</sup> and by the RGibbs tool for the two



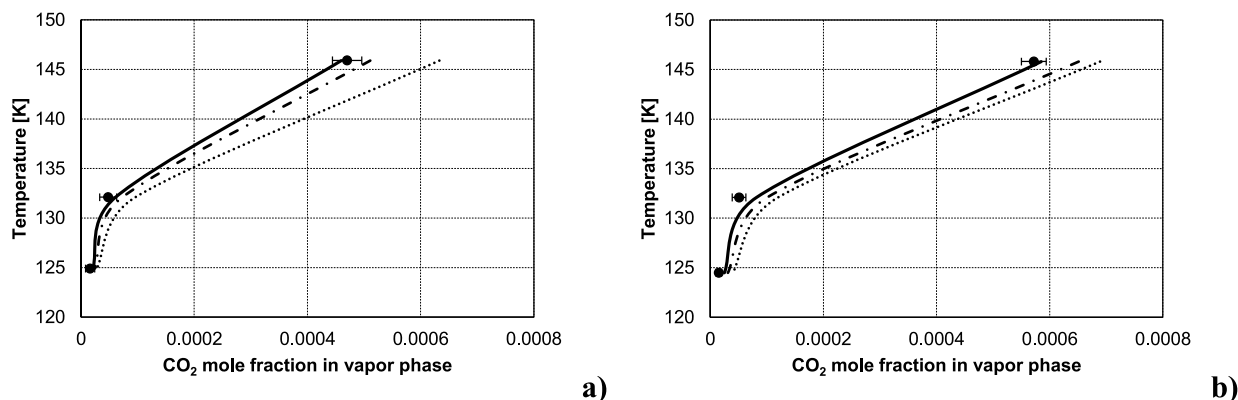


**Figure 13.** CO<sub>2</sub> mole fraction in the vapor phase at SLVE conditions for the CO<sub>2</sub>–CH<sub>4</sub>–N<sub>2</sub> system: comparison between the results obtained with the proposed algorithm (solid line), by simulation of RGibbs in Aspen Plus V9.0<sup>42</sup> (dashed and dotted line), and by Riva and Stringari<sup>14</sup> (dotted line). Two mixtures are considered: (a, Mixture 1) 2 mol % CO<sub>2</sub>, 58 mol % CH<sub>4</sub>, 40 mol % N<sub>2</sub>; (b, Mixture 2) 2 mol % CO<sub>2</sub>, 79 mol % CH<sub>4</sub>, 19 mol % N<sub>2</sub>.

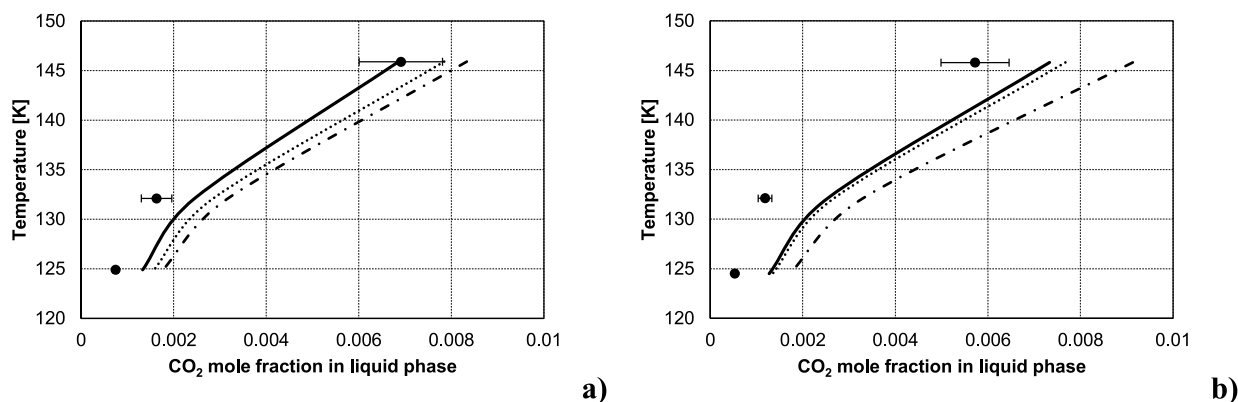


**Figure 14.** CO<sub>2</sub> mole fraction in the liquid phase at SLVE conditions for the CO<sub>2</sub>–CH<sub>4</sub>–N<sub>2</sub> system: comparison between the results obtained with the proposed algorithm (solid line), by simulation of RGibbs in Aspen Plus V9.0<sup>42</sup> (dashed and dotted line), and by Riva and Stringari<sup>14</sup> (dotted line). Two mixtures are considered: (a, Mixture 1) 2 mol % CO<sub>2</sub>, 58 mol % CH<sub>4</sub>, 40 mol % N<sub>2</sub>; (b, Mixture 2) 2 mol % CO<sub>2</sub>, 79 mol % CH<sub>4</sub>, 19 mol % N<sub>2</sub>.

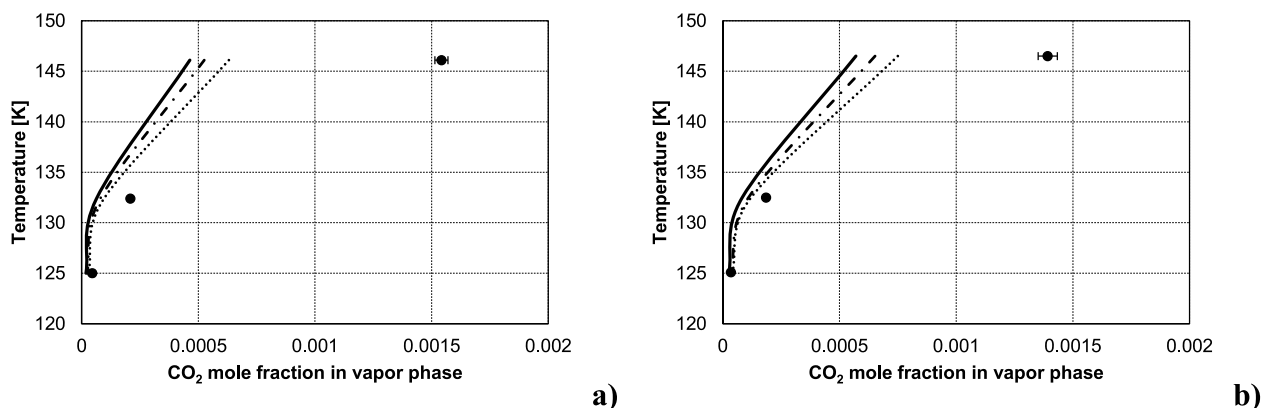


**Figure 15.** CO<sub>2</sub> mole fraction in the vapor phase at SLVE conditions for the CO<sub>2</sub>–CH<sub>4</sub>–N<sub>2</sub>–O<sub>2</sub> system: comparison between the results obtained with the proposed algorithm (solid line), by simulation of RGibbs in Aspen Plus V9.0<sup>42</sup> (dashed and dotted line), and by Riva and Stringari<sup>14</sup> (dotted line). Two mixtures are considered: (a, Mixture 1) 2 mol % CO<sub>2</sub>, 58 mol % CH<sub>4</sub>, 31 mol % N<sub>2</sub>, 9 mol % O<sub>2</sub>; (b, Mixture 2) 2 mol % CO<sub>2</sub>, 79 mol % CH<sub>4</sub>, 15 mol % N<sub>2</sub>, 4 mol % O<sub>2</sub>.

mixtures. It is possible to observe that the proposed algorithm (solid line) shows the best performances among the three, since the other two approaches tend to overestimate the CO<sub>2</sub> content in both fluid phases at SLVE conditions.

**4.3. The CO<sub>2</sub>–CH<sub>4</sub>–N<sub>2</sub>–O<sub>2</sub> System.** Riva and Stringari<sup>14</sup> presented SLVE data for two mixtures consisting of CO<sub>2</sub>, CH<sub>4</sub>,

N<sub>2</sub>, and O<sub>2</sub>, and applied the same calculation approach used for the ternary mixture without oxygen (described in the previous section) to SLVE calculations for these two quaternary mixtures. Such mixtures are characterized by the same content of CO<sub>2</sub> and CH<sub>4</sub> as the two ternary mixtures in which O<sub>2</sub> was not present, and the percentage of N<sub>2</sub> is

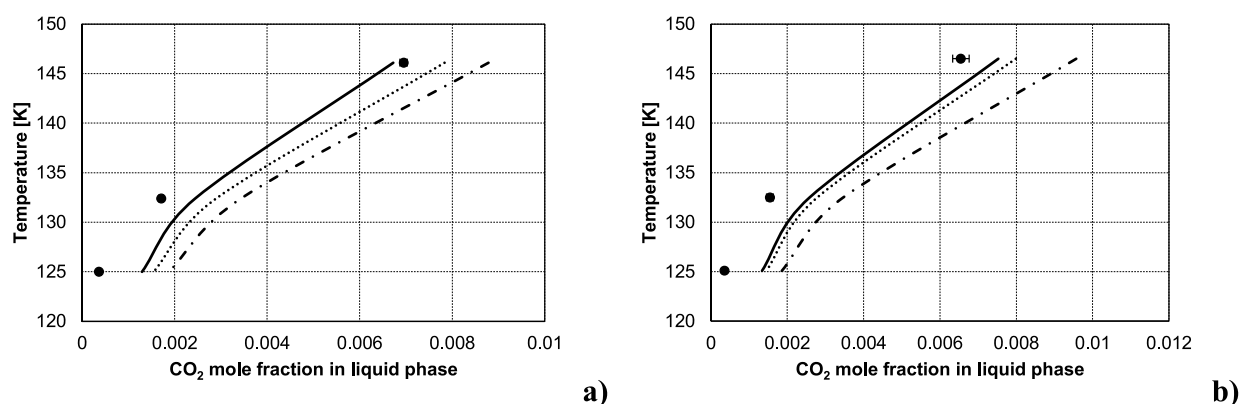


**Figure 16.** CO<sub>2</sub> mole fraction in the liquid phase at SLVE conditions for the CO<sub>2</sub>–CH<sub>4</sub>–N<sub>2</sub>–O<sub>2</sub> system: comparison between the results obtained with the proposed algorithm (solid line), by simulation of RGiBbs in Aspen Plus V9.0<sup>42</sup> (dashed and dotted line), and by Riva and Stringari<sup>14</sup> (dotted line). Two mixtures are considered: (a, Mixture 1) 2 mol % CO<sub>2</sub>, 58 mol % CH<sub>4</sub>, 31 mol % N<sub>2</sub>, 9 mol % O<sub>2</sub>; (b, Mixture 2) 2 mol % CO<sub>2</sub>, 79 mol % CH<sub>4</sub>, 15 mol % N<sub>2</sub>, 4 mol % O<sub>2</sub>.

consequently decreased in favor of O<sub>2</sub>. The experimental data and the calculation results obtained with their approach, as well as with the two taken into account in this work, are illustrated in Figures 15 and 16.

It is possible to notice that, according to the experimental values, the CO<sub>2</sub> mole fraction in the vapor phase at SLVE increases when some nitrogen is replaced by oxygen (Figure 15 vs Figure 13), but this phenomenon is not correctly predicted by any of the three approaches. The availability of more experimental data for this quaternary mixture will certainly help to better understand the reason for these discrepancies.

The mole fraction of CO<sub>2</sub> in the liquid phase is overestimated by the different approaches, as can be seen in Figure 16, with the exception of the point at the highest temperature for the results obtained with the proposed approach, which performs better than the other two approaches. This behavior may be explained considering that the parameters used by the thermodynamic models for the fluid phases (e.g., the binary interaction parameters,  $k_{ij}$ s, for the Peng–Robinson EoS) are optimized for the vapor–liquid equilibrium at conditions different from the ones at which they are in equilibrium with solid CO<sub>2</sub>. Though the three approaches make use of different thermodynamic models and are based on the implementation of different algorithms (Rachford–Rice method coupled to a phase stability analysis as for the proposed algorithm; Gibbs energy minimization as for the RGiBbs tool; classical approach based on the isofugacity condition as for the approach adopted by Riva and Stringari<sup>14</sup>), they are consistent with each other. Therefore, as also stated by the authors presenting the experimental data for the quaternary mixture, “more experimental studies are suggested to provide a full description of the system behavior as a function of temperature, pressure, and nitrogen and/or oxygen mole fraction”.<sup>14</sup>

## 5. CONCLUSIONS

This work deals with phase equilibria in the presence of solid CO<sub>2</sub> for mixtures of interest in the fields of natural gas purification and biogas/landfill gas upgrading. Experimental data for solid–vapor equilibria and solid–liquid–vapor equilibria available in the literature are first reviewed, reporting the type of measurements to which they refer for the CO<sub>2</sub>–CH<sub>4</sub> binary mixture, the CO<sub>2</sub>–CH<sub>4</sub>–N<sub>2</sub> ternary mixture, and the CO<sub>2</sub>–CH<sub>4</sub>–N<sub>2</sub>–O<sub>2</sub> quaternary mixture. Such data have

been used for the validation of a thermodynamic calculation approach that allows coupling a phase stability analysis with isothermal–isobaric flash computations in multiphase systems at given temperature, pressure, and their global composition without knowing *a-priori* the number and the type of phases present at equilibrium. The algorithm can be applied to calculations of phase diagrams involving the liquid and vapor fluid phases and a solid phase, which consists of pure CO<sub>2</sub>, and will be further developed in the future to account for the presence of more phases, so to allow the application to more complex systems, such as those that may exhibit a miscibility gap and lead to liquid–liquid equilibria at certain temperature and pressure conditions.

The proposed algorithm has turned out to satisfactorily predict the behavior of the mixtures taken into account, with an average absolute deviation not higher than 1.3% when considering, for example, the calculation of CO<sub>2</sub> frost point temperature in the binary mixture with methane. In some cases, especially for the quaternary mixture, the results are in good agreement with those obtained with other approaches based on different models, but to a lesser extent with the few available experimental data. To better assess the reliability of the proposed algorithm, more experimental studies are needed to enrich the database, especially for multicomponent mixtures involving nonhydrocarbon compounds in addition to carbon dioxide and methane. Nitrogen and oxygen are two of them, which can be found in natural gas and in biogas/landfill gas. Since CO<sub>2</sub> has to be separated from these gases to produce a pipeline-quality gas or liquefied natural gas (LNG)/liquefied biomethane (bioLNG), and some processes for this purpose are operated at conditions where solid CO<sub>2</sub> may form, process engineers should know at which conditions the process must be operated if the formation of dry ice must be avoided. For this, the availability of more experimental data (e.g., at higher concentrations of nitrogen, which can reach 40 mol %<sup>5</sup> and larger values in natural gas or associated gas, at concentrations of CO<sub>2</sub> higher than 20 mol %—the maximum value for which SVE and/or SLVE data are now available in the literature for the ternary and quaternary mixture taken into account in this work—and at pressures higher than 20 bar at which some CO<sub>2</sub> low-temperature/cryogenic separation processes are operated) could allow a better description of the system thermodynamic behavior as a function of temperature, pressure, and

composition and could, consequently, allow a better process design.

## ■ ASSOCIATED CONTENT

### SI Supporting Information

The Supporting Information is available free of charge at <https://pubs.acs.org/doi/10.1021/acs.jced.1c00330>.

Details on (i) the experimental literature data used for validation of the proposed algorithm; (ii) the properties of the components taken into account in this work and the theoretical background for the algorithm proposed for simultaneous multiphase flash and stability analysis calculations including solid CO<sub>2</sub>. (PDF)

## ■ AUTHOR INFORMATION

### Corresponding Author

**Giorgia De Guido** – GASP—Group on Advanced Separation Processes & GAS Processing, Dipartimento di Chimica, Materiali e Ingegneria Chimica “Giulio Natta”, Politecnico di Milano, I-20133 Milano, Italy; [orcid.org/0000-0003-2018-4452](https://orcid.org/0000-0003-2018-4452); Phone: +39 02 2399 3260; Email: [giorgia.deguido@polimi.it](mailto:giorgia.deguido@polimi.it); Fax: +39 02 2399 3280

### Author

**Elvira Spatolisano** – GASP—Group on Advanced Separation Processes & GAS Processing, Dipartimento di Chimica, Materiali e Ingegneria Chimica “Giulio Natta”, Politecnico di Milano, I-20133 Milano, Italy; [orcid.org/0000-0002-3316-0487](https://orcid.org/0000-0002-3316-0487)

Complete contact information is available at: <https://pubs.acs.org/doi/10.1021/acs.jced.1c00330>

### Notes

The authors declare no competing financial interest.

## ■ REFERENCES

- (1) Babar, M.; Bustam, M. A.; Ali, A.; Maulud, A. S.; Shafiq, U.; Mukhtar, A.; Shah, S. N.; Maqsood, K.; Mellon, N.; Shariff, A. M. Thermodynamic data for cryogenic carbon dioxide capture from natural gas: a review. *Cryogenics* **2019**, *102*, 85–104.
- (2) Pellegrini, L. A.; Langè, S.; Baccanelli, M.; De Guido, G., Techno-Economic Analysis of LNG Production Using Cryogenic Vs Conventional Techniques for Natural Gas Purification. In Offshore Mediterranean Conference and Exhibition, Offshore Mediterranean Conference: Ravenna, Italy, 2015.
- (3) Pellegrini, L. A.; De Guido, G.; Langè, S. Biogas to liquefied biomethane via cryogenic upgrading technologies. *Renewable Energy* **2018**, *124*, 75–83.
- (4) Pellegrini, L. A.; De Guido, G.; Langè, S.; Moiola, S.; Picutti, B.; Vergani, P.; Franzoni, G.; Brignoli, F., The Potential of a New Distillation Process for the Upgrading of Acid Gas. In Abu Dhabi International Petroleum Exhibition & Conference (ADIPEC); Society of Petroleum Engineers: Abu Dhabi, UAE, 2016.
- (5) De Guido, G.; Messinetti, F.; Spatolisano, E. Cryogenic Nitrogen Rejection Schemes: Analysis of Their Tolerance to CO<sub>2</sub>. *Ind. Eng. Chem. Res.* **2019**, *58* (37), 17475–17488.
- (6) Pikaar, M. J. A study of phase equilibria in hydrocarbon-CO<sub>2</sub> systems. Ph.D. Thesis, Imperial College of Science and Technology, London, 1959.
- (7) Le, T. T.; Trebble, M. A. Measurement of carbon dioxide freezing in mixtures of methane, ethane, and nitrogen in the solid–vapor equilibrium region. *J. Chem. Eng. Data* **2007**, *52* (3), 683–686.
- (8) Agrawal, G.; Laverman, R. Phase behavior of the methane-carbon dioxide system in the solid-vapor region. In *Advances in Cryogenic Engineering*; Springer, 1995; pp 327–338.
- (9) Zhang, L.; Burgass, R.; Chapoy, A.; Tohidi, B.; Solbraa, E. Measurement and Modeling of CO<sub>2</sub> Frost Points in the CO<sub>2</sub>–Methane Systems. *J. Chem. Eng. Data* **2011**, *56* (6), 2971–2975.
- (10) De Guido, G.; Fogli, M. R.; Pellegrini, L. A. Effect of Heavy Hydrocarbons on CO<sub>2</sub> Removal from Natural Gas by Low-Temperature Distillation. *Ind. Eng. Chem. Res.* **2018**, *57* (21), 7245–7256.
- (11) Xiong, X.; Lin, W.; Jia, R.; Song, Y.; Gu, A. Measurement and calculation of CO<sub>2</sub> frost points in CH<sub>4</sub>+ CO<sub>2</sub>/CH<sub>4</sub>+ CO<sub>2</sub>+ N<sub>2</sub>/CH<sub>4</sub>+ CO<sub>2</sub>+ C<sub>2</sub>H<sub>6</sub> mixtures at low temperatures. *J. Chem. Eng. Data* **2015**, *60* (11), 3077–3086.
- (12) Shen, T.; Gao, T.; Lin, W.; Gu, A. Determination of CO<sub>2</sub> solubility in saturated liquid CH<sub>4</sub>+ N<sub>2</sub> and CH<sub>4</sub>+ C<sub>2</sub>H<sub>6</sub> mixtures above atmospheric pressure. *J. Chem. Eng. Data* **2012**, *57* (8), 2296–2303.
- (13) Gao, T.; Shen, T.; Lin, W.; Gu, A.; Ju, Y. Experimental determination of CO<sub>2</sub> solubility in liquid CH<sub>4</sub>/N<sub>2</sub> mixtures at cryogenic temperatures. *Ind. Eng. Chem. Res.* **2012**, *51* (27), 9403–9408.
- (14) Riva, M.; Stringari, P. Experimental study of the influence of nitrogen and oxygen on the solubility of solid carbon dioxide in liquid and vapor methane at low temperature. *Ind. Eng. Chem. Res.* **2018**, *57* (11), 4124–4131.
- (15) Donnelly, H. G.; Katz, D. L. Phase equilibria in the carbon dioxide–methane system. *Ind. Eng. Chem.* **1954**, *46* (3), 511–517.
- (16) Sterner, C., Phase equilibria in the CO<sub>2</sub>–methane systems. In *Advances in Cryogenic Engineering*; Springer, 1961; pp 467–474.
- (17) Davis, J.; Rodewald, N.; Kurata, F. Solid-liquid-vapor phase behavior of the methane-carbon dioxide system. *AIChE J.* **1962**, *8* (4), 537–539.
- (18) Im, K. U.; Kurata, F. Phase equilibrium of carbon dioxide and light paraffins in presence of solid carbon dioxide. *J. Chem. Eng. Data* **1971**, *16* (3), 295–299.
- (19) Brewer, J.; Kurata, F. Freezing points of binary mixtures of methane. *AIChE J.* **1958**, *4* (3), 317–318.
- (20) Haufe, S.; Tieze, G.; Muller, H. Solubility of solid carbon-dioxide in a mixture of methane and nitrogen. *Chemische Technik* **1972**, *24* (10), 619.
- (21) De Guido, G.; Langè, S.; Moiola, S.; Pellegrini, L. A. Thermodynamic method for the prediction of solid CO<sub>2</sub> formation from multicomponent mixtures. *Process Saf. Environ. Prot.* **2014**, *92* (1), 70–79.
- (22) Gupta, A. K. Steady state simulation of chemical processes. Ph.D. Thesis, University of Calgary, Calgary, 1990.
- (23) Gautam, R.; Seider, W. D. Computation of phase and chemical equilibrium: Part I. Local and constrained minima in Gibbs free energy. *AIChE J.* **1979**, *25* (6), 991–999.
- (24) Michelsen, M. L. The isothermal flash problem. Part I. Stability. *Fluid Phase Equilib.* **1982**, *9* (1), 1–19.
- (25) Michelsen, M. L. The isothermal flash problem. Part II. Phase-split calculation. *Fluid Phase Equilib.* **1982**, *9* (1), 21–40.
- (26) Michelsen, M. L. Multiphase isenthalpic and isentropic flash algorithms. *Fluid Phase Equilib.* **1987**, *33* (1–2), 13–27.
- (27) Wu, J.-S.; Bishnoi, P. An algorithm for three-phase equilibrium calculations. *Comput. Chem. Eng.* **1986**, *10* (3), 269–276.
- (28) Castier, M.; Rasmussen, P.; Fredenslund, A. Calculation of simultaneous chemical and phase equilibria in nonideal systems. *Chem. Eng. Sci.* **1989**, *44* (2), 237–248.
- (29) Gupta, A. K.; Bishnoi, P. R.; Kalogerakis, N. Simultaneous multiphase isothermal/isenthalpic flash and stability calculations for reacting/non-reacting systems. *Gas Sep. Purif.* **1990**, *4* (4), 215–222.
- (30) Gupta, A. K.; Bishnoi, P. R.; Kalogerakis, N. A method for the simultaneous phase equilibria and stability calculations for multiphase reacting and non-reacting systems. *Fluid Phase Equilib.* **1991**, *63* (1–2), 65–89.
- (31) Ballard, A.; Sloan, E., Jr The next generation of hydrate prediction: Part III. Gibbs energy minimization formalism. *Fluid Phase Equilib.* **2004**, *218* (1), 15–31.

- (32) Segtovich, I. S. V.; Barreto, A. G., Jr; Tavares, F. W. Simultaneous multiphase flash and stability analysis calculations including hydrates. *Fluid Phase Equilib.* **2016**, *413*, 196–208.
- (33) Tang, L.; Li, C.; Lim, S. Solid–Liquid–Vapor Equilibrium Model Applied for a CH<sub>4</sub>–CO<sub>2</sub> Binary Mixture. *Ind. Eng. Chem. Res.* **2019**, *58* (39), 18355–18366.
- (34) Jäger, A.; Span, R. Equation of state for solid carbon dioxide based on the Gibbs free energy. *J. Chem. Eng. Data* **2012**, *57* (2), 590–597.
- (35) De Guido, G.; Pellegrini, L. Application of Conventional and Novel Low-temperature CO<sub>2</sub> Removal Processes to Lng Production at Different CO<sub>2</sub> Concentrations in Natural Gas. *Chem. Eng. Trans.* **2019**, *74*, 853–858.
- (36) Qyum, M. A.; Haider, J.; Qadeer, K.; Valentina, V.; Khan, A.; Yasin, M.; Aslam, M.; De Guido, G.; Pellegrini, L. A.; Lee, M. Biogas to liquefied biomethane: Assessment of 3P's—Production, processing, and prospects. *Renewable Sustainable Energy Rev.* **2020**, *119*, 109561.
- (37) Ballard, A. L. A non-ideal hydrate solid solution model for a multi-phase equilibria program. Ph.D. Thesis, Colorado School of Mines, 2002.
- (38) Peng, D.-Y.; Robinson, D. B. A new two-constant equation of state. *Ind. Eng. Chem. Fundam.* **1976**, *15* (1), 59–64.
- (39) Jensen, M. J.; Russell, C. S.; Bergeson, D.; Hoeger, C. D.; Frankman, D. J.; Bence, C. S.; Baxter, L. L. Prediction and validation of external cooling loop cryogenic carbon capture (CCC-ECL) for full-scale coal-fired power plant retrofit. *Int. J. Greenhouse Gas Control* **2015**, *42*, 200–212.
- (40) Friend, D. G.; Ely, J. F.; Ingham, H. Thermophysical properties of methane. *J. Phys. Chem. Ref. Data* **1989**, *18* (2), 583–638.
- (41) Pellegrini, L. A.; De Guido, G.; Ingham, S. In *Thermodynamic Framework for Cryogenic Carbon Capture*, 30th European Symposium on Computer Aided Process Engineering (ESCAPE30), Milan, Italy, May 24–27, 2020; Elsevier B.V: Milan, Italy, 2020.
- (42) AspenTech *Aspen Plus*; AspenTech: Burlington (MA), United States, 2016.